Physics – Uspekhi **39** (6) 547 – 572 (1996)

REVIEWS OF TOPICAL PROBLEMS PACS numbers: 43.35. Rw, 75.30.Ds, 75.50.Gg

Magnetoacoustics of rare-earth orthoferrites

V D Buchel'nikov, N K Dan'shin, L T Tsymbal, V G Shavrov

Contents

Abstract. Experimental and theoretical work on the magnetoacoustics of rare-earth orthoferrites near reorientation phase transitions (RPTs) is reviewed. The temperature and field dependence of magnetoresonant soft-mode frequencies and of the sound velocity and attenuation near various RPTs, as obtained by RF and ultrasonic spectroscopy, are given. A spin-wave approximation theoretical analysis of orthoferrite magnetoacoustics is presented, accounting as fully as possible for interactions between all the subsystems involved, including the ordered ferrous, elastic, paramagnetic rare-earth, and dipole (electromagnetic) subsystems. The origin of energy gaps in the spin-wave spectrum is discussed in detail, as are the ultrasonic dispersion, propagation velocity, and attenuation changes at RPT points. The energy gaps measured and the sound velocity behaviour observed are shown to result from the interaction of the orthoferrite subsystems. In most cases experimental data agree well with theoretical predictions.

1. Introduction

The magnetoelastic (ME) coupling is among relatively weak interactions in magnetic crystals. In some cases, however — close to a reorientation phase transition (RPT), for example, where the total magnetic anisotropy energy drops to zero — it is this coupling which dominates many of the properties of magnetically ordered substances. Strong effects of the relatively weak ME coupling are still the subject of continuing interest. This is true, in particular, for a dynamical manifestation of magnetoelasticity — the magnetoacoustics of magnetic materials.

Such a large effect of the ME coupling on the dynamics of a magnetic material was first reported in the 1963 works of Rudashevsky and Shalnikova [1] and Tasaki and Iida [2] on hematite, an antiferromagnet with an 'easy plane' anisotropy. In investigating the dependence of the low-frequency mode ω_0 on the basal-plane magnetic field H it was found that on approaching the RPT with respect to the field H ($H \to 0$), the frequency ω_0 acquires a large additional contribution due to the ME coupling, thus

$$\omega_0^2 = \omega_0^{*2} + \omega_\Delta^2 .$$

Here ω_0^* is the usual magnetic-anisotropy magnetic-field contribution. Since there is virtually no basal-plane anisotropy in hematite, we have

$$\omega_0^{*2} = g^2 H(H + H_D) ,$$

where H_D is the Dzyaloshinskiĭ field, and g is the spectroscopic splitting factor. The additional second term represents a magnetoelastic gap in the quasimagnon spectrum [1 – 5]. For easy-plane antiferromagnets it is expressed in terms of the effective uniform-exchange and magnetostriction fields by

$$\omega_\Delta = \omega_E \omega_{me} = g^2 H_E H_{me} .$$

Along with the ME gap effect, in the RPT region a strong deformation of the quasiphonon mode occurs, so that at

V D Buchel'nikov Chelyabinsk State University, 454136 Chelyabinsk, Russia. Tel. (7-351) 242 03 47
N K Dan'shin, L T Tsymbal Donetsk Physical-Technical Institute, National Academy of Sciences of Ukraine, 340114 Donetsk, Ukraine Tel. (7-062) 255 72 26
V G Shavrov Institute of Radio Engineering and Electronics, Russian Academy of Sciences, 103907 Moscow, Russia
Tel. (7-095) 203 24 26

Received 24 July 1995, revised 9 January 1996
Uspekhi Fizicheskikh Nauk **166** (6) 585 – 612 (1996)
Translated by E G Strel'chenko; edited by S D Danilov

small enough quasimomenta k the dispersion of this mode may change from linear to quadratic (see Ref. [6] and references therein). This, in turn, leads to a significant decrease in the velocity of sound with approaching the RPT (in the theoretical limit, to zero at the exact transition point as $k \to 0$).

The appearance of the ME gap in the quasimagnon mode near the RPT is related to the magnetic moment and crystal lattice vibrations being oppositely phased. An analogue of such vibrations is optical lattice vibrations. To nonactivated quasielastic low-frequency vibrations there correspond in-phase magnetic-moment and lattice vibrations, an analogue of which is the acoustic vibrations. Due to the ME coupling, the magnons make the phonons 'heavier', and it is this effect which leads to a decrease in the sound velocity. It has long been thought that the ME coupling is the only contributor to the spin-wave gap and is therefore readily amenable to experimental determination, in spite of its being small. In some magnetic materials, however, it has been found not to dominate the quasi-spin gap at the RPT point. One example is the rare-earth orthoferrites (REOFs), a class of relatively complex magnetic materials which are widely used in the study of ME effects.

Because the REOFs have two magnetic subsystems, a ferrous and a rare-earth, and because these subsystems have greatly different properties, interact with one another and change their effective anisotropy constants with temperature, field, or elastic stress, a whole series of RPTs take place in these materials. These have provided a rich experimental basis for both the comparative study of ME effects (particularly by replacing the rare-earth ions) and the development of a general theory [6]. A detailed, specifically REOF coupled vibration analysis [7] included only two subsystems, ferrous and elastic, and yielded quantitative estimates which disagreed with experiment. In fact, each subsequent investigation of the problem added experimental data which proved inexplicable in terms of the existing theory. The present article reviews and summarises the views and ideas dominating the subject, although it cannot of course make a claim for the final word in the understanding of this phenomenon, so multifaceted in its manifestations and so important from the practical point of view.

In recent years, extensive experimental work on certain REOFs in the RPT region has suggested new conclusions about the ME effects on the dynamics of magnetic materials (see, e.g., Refs [8 – 19]). It has been realised that the presence of activation in the magnon spectrum at second-order RPTs is in itself an insufficient proof that the dynamic coupling of elastic and spin waves is a dominant contributor. Rather, as we shall see, it can be argued that the experimentally observed gaps in the spectra of magnetoresonant soft modes cannot be identified with the magnetoelastic gap, that is, cannot be interpreted entirely in terms of the action the elastic subsystem exerts on the magnetic one (as was done in Ref. [7]). In fact, apart from the dipole contribution to the observed values of REOF gaps (which was also predicted in Ref. [7]), it has been found that, in general, a number of interactions must be added to the picture. Another finding has been a significant disagreement between theory and experiment on the behaviour (specifically, the magnitude of change) of the sound velocity in the RPT region. Until recently, sound velocity decreases of only 0.1 to 3% have been reported [20 – 24, 12] for RPTs in various orthoferrites — which is small compared to theoretical predictions [7] — and only erbium orthoferrite near the low-temperature RPT point of ~ 4 K first revealed a 25% dip [14, 15], a huge effect as far as the REOFs are concerned. This fact came as a final stimulus for the revision of the existing theoretical views on the magnetoacoustics of orthoferrites. The present day view of this problem is that a full description of the spectrum of coupled vibrations in a REOF requires that four subsystems, namely, the magnetically ordered ferrous, elastic, paramagnetic rare-earth, and dipole (or electromagnetic), be included [25 – 29]. Earlier work (see, e.g., a review [30] and references therein) has demonstrated the importance of the paramagnetic rare-earth (ME uncoupled) subsystem for the calculation of the spin wave spectrum. To summarise, the quasimagnon activation (frequency gap) and the change of the quasiphonon dispersion at the RPT point are, in a way, a result — and a measure — of the dynamic interactions of the vibrational subsystems mentioned above. Although formulated specifically for the REOFs, this conclusion may be extended to other complex, magnetically ordered materials. Unfortunately, however, no experimental test is available by means of which the ME contribution to the absolute value of the measured gap can be separated from other contributions which, although different in nature, are similar in their manifestation. Our task here is to estimate the role of the ME coupling in the observed effects by taking into account as fully as possible both the factors that form and those that mask this coupling. More generally, our aim is to elucidate the theoretically predicted mutual influence of the subsystems considered [6, 7, 25 – 29]. It is not out of place to note that previous theory employed the ordinary condition of constancy for the absolute sublattice magnetisations, $\mathbf{M}_n^2 = M_0^2 = \text{const}$ ($\mathbf{M}_n$ is the nth sublattice magnetisation, $M_0 = |\mathbf{M}_n|$). There is experimental and theoretical evidence, however, to show (see, e.g., Refs [31 – 34]) that a departure from this condition leads to the excitation of relaxational modes which also contribute to the magnitude of the observed gaps. This theory has been tested and confirmed in submillimetre experiments on $YFeO_3$, $DyFeO_3$, and Fe_3BO_6 near RPTs induced by a strong magnetic field. These studies are mentioned only briefly here, just to illustrate that an original assumption (in this case, about the role of the longitudinal susceptibility in a strong magnetic field at high temperatures) may produce an additional contribution to the gap. In the discussion section we will consider in more detail the gap formation mechanism of Refs [31 – 34] in order to show that (contrary to the recent view) it is not at all alternative to the mechanisms discussed in the present review. In the following we will assume, as is traditional, that the magnetic sublattices are saturated at reorientation temperatures considered, and that longitudinal magnetisation vibrations may be neglected.

1.1 Objects of the study

We start with some of the general properties of the materials under study. A characteristic feature of the REOFs (space group D_{2h}^{16}) is the presence of two magnetic subsystems, rare-earth and ferrous. At $T = T_{N1} \lesssim 620 - 740$ K the magnetic d subsystem of the REOF iron ions orders into a noncollinear, antiferromagnetic four-lattice structure. Of the two optical (~ 500 cm^{-1}) and two acoustic (~ 10 cm^{-1}) modes of this structure, only the latter — low-frequency — modes will be discussed in the following. In such a two-sublattice model, the magnetic structure of iron corresponds to the irreducible representation $\Gamma_4(G_x, F_z)$, where G_x and F_z are the components of the antiferromagnetism $\mathbf{G} = (\mathbf{M}_1 - \mathbf{M}_2)/2M_0$ and

ferromagnetism $\mathbf{F} = (\mathbf{M}_1 + \mathbf{M}_2)/2M_0$ vectors, respectively. One of the acoustic branches is excited by a uniform RF field $\mathbf{h} \perp \mathbf{F}$ (quasiferromagnetic or σ mode), and the other, by $\mathbf{h} \parallel \mathbf{F}$ (quasiantiferromagnetic, or γ mode). Their respective frequencies depend on the anisotropies in the **ac** (xz) and **ab** (xy) planes of the crystal [35] (the crystalline axes **a**, **b**, and **c** lie along the x, y, and z coordinate axes, respectively). The ions of the rare-earth f subsystem at temperatures $T > 10$ K (or lower) are in the paramagnetic state. Direct electronic transitions within the basic multiplet have been found in many REOFs and are being widely studied using the submillimetre spectroscopy technique [30] (the usual EPR effect in the effective field of iron in the crystal field). Along with the direct electronic transitions (R) there is a resonance branch (r), whose symmetry is identical to that of the AFMR ordered iron σ mode. Since the rare-earth ions are under the ordering influence of iron, the resonant rare-earth modes can be treated as collective excitations within the paramagnetic f subsystem and, in the approximation we use, can also be described by a two-sublattice model with ferromagnetism ($\mathbf{f} = (\boldsymbol{\sigma}_1 + \boldsymbol{\sigma}_2)/2$) and antiferromagnetism ($\mathbf{c} = (\boldsymbol{\sigma}_1 - \boldsymbol{\sigma}_2)/2$) vectors, where $\sigma_{1,2}$ are the mean values of the rare-earth sublattice Pauli matrices. The spectrum of magnetic vibrations then consists of four branches, two (σ, γ) arising from the vibrations of the d subsystem, and two (R, r), from the vibrations of the f subsystem [36, 37].

As noted earlier, a characteristic feature of the compounds we are considering is the occurrence of various types of RPTs due to the anisotropic temperature-dependent d–f interaction [38]. The most common type of spin reorientation is

$$\Gamma_4(G_x, F_z) \rightarrow \Gamma_{24}(G_{x,z}, F_{x,z}) \rightarrow \Gamma_2(G_z, F_x)\,,$$

with the vectors **F** and **G** smoothly rotating in the **ac** crystal plane. The temperature interval where the reorientation takes place is ~ 10 K, its boundaries at temperatures T_1 and T_2 being the second-order phase transition points (we let $T_1 > T_2$, to be specific; at temperatures $T_{N1} > T > T_1$, the Γ_4 phase exists). Such a reorientation is realised in the orthoferrites of thulium, erbium, ytterbium, samarium, neodymium, and, in a somewhat modified form, in $HoFeO_3$. In $ErFeO_3$ and $HoFeO_3$, the $\Gamma_2 - \Gamma_{12}$ RPT also occurs. Note that since the d–d exchange is three orders of magnitude stronger than the d–f and f–f interactions, the saturation of the magnetic subsystem of iron near the reorientation temperatures $T_1, T_2 \sim 100$ K appears to be quite a viable assumption.

Near an RPT, either the iron or the rare-earth mode (for the $\Gamma_2 - \Gamma_4$ case, the σ and r mode, respectively) can be a soft one, depending on the initial ratio of the frequencies of the d and f subsystems, which in turn is determined by the specific properties of the rare-earth ion in question [36, 37]. In contrast to early views, whether the rare-earth ion is of the Kramers or non-Kramers type (has an odd or even number of 4f electrons) is immaterial because, analogous to the low-frequency transitions within the main doublet in a Kramers ion, in non-Kramers ions quasidoublets with low transition frequencies may occur. Near the reorientation point, owing to the intersection of and strong coupling between the resonant modes, both the f and d mode may be strong in a particular orthoferrite. Indeed, for modes with close frequencies and the same symmetry the distinction between iron and rare-earth types is to a large extent irrelevant, and one can only speak of which of the magnetic subsystems dominates the observed effects. It is important to note that although the rare-earth ions are in the paramagnetic state, sometimes they play a central role in determining the dynamics of a magnetic material in the RPT region.

Thus, the occurrence of similar $\Gamma_4 - \Gamma_{24} - \Gamma_2$ transitions in all the REOFs studied enables one, by employing the details of the observed acoustic anomalies, gap magnitudes, spectral characteristics of soft magnetic modes, etc., to carry out a comparative analysis of the near-RPT dynamics, to examine its dependence on various relevant factors, and to estimate the actual role of the ME coupling in the formation of the magnon gap. Of particular interest, in connection with the study of ME effects, are experiments in which, on the same REOF, both the magnon and the phonon branches are studied. With this in mind, we present below a detailed analysis of experimental data on four REOFs, $ErFeO_3$ and $YbFeO_3$ with Kramers f ions, and $TmFeO_3$ and $HoFeO_3$ with non-Kramers ions, in which the magnetic resonance and ultrasonic anomalies at $\Gamma_2 - \Gamma_{24} - \Gamma_4$ RPTs have been investigated. For completeness, we add RF measurements on $NdFeO_3$ and $SmFeO_3$, materials in which only the spin wave mode has thus far been studied.

1.2 Experimental technique

An important methodological point to make about the experiments reviewed is that they are mainly associated with spontaneous transitions with respect to temperature. First, this makes it unnecessary to bother each time about the magnetic field contribution to the observed effects, and to a certain extent justifies the neglect of the longitudinal susceptibility, which increases in a strong field [31–34]. Second, temperature RPTs make it easier to compare the experimental data with the existing theory and with the widely quoted submillimetre data [30], also obtained for spontaneous transitions. Third, and perhaps most important, this technique avoids the unpleasant field-experiment feature that the field may distort the original magnetic structure of the existing phases yielding (even when only slightly away from the crystal axes) a too large value for the measured gap at the RPT induced [39, 40]. The direct method of restoring soft magnon and phonon spectra near RPTs from signal records made during the temperature scanning has turned out to be the most effective as well as a very convenient technique to compare experimental data with theory. However, whenever it was of interest, a check was made on the effect of the magnetic field (fixed or scanning) on measurements performed at spontaneous RPTs.

Resonance experiments were made with a wideband (14–79 GHz) direct-gain spectrometer. Absorption signals were recorded at fixed frequencies during temperature (magnetic field) scanning. From the set of such records, the corresponding dependence of the soft magnetic-resonance mode frequency was constructed. The polarisation of the RF magnetic field **h** was chosen in accordance with the symmetry of the vibrations under study.

Acoustic studies were conducted using a pulsed ultrasonic spectrometer. Sound vibrations were excited by a niobium-lithium resonance piezotransducer at frequencies $\nu = \omega/2\pi$ between 25 and 250 MHz. To measure relative sound velocity changes, a phase sensitive technique was used. The polarisation of the displacement vector **u** of the transversal ultrasonic wave was determined by the symmetry conditions for the excitation of active ultrasonic modes associated with soft

magnon modes. To facilitate the comparison of results from various REOFs, an active wave propagating along the **c** axis was taken. For example, for the $\Gamma_2-\Gamma_4$ transitions, this was the wave with the wave vector $\mathbf{k} \parallel \mathbf{c}$ and with $\mathbf{u} \parallel \mathbf{a}$ (although the shear wave with $\mathbf{k} \parallel \mathbf{a}$, $\mathbf{u} \parallel \mathbf{c}$ is also active).

Single crystalline samples were used: for resonance measurements, 0.8-mm-diameter spheres, for ultrasonic measurements, rounded-edge cylinders (disks), 4 mm in diameter and 1.5 – 6 mm thick.

2. Experimental study of the dynamics of rare-earth orthoferrites near reorientation phase transitions

2.1 Magnetoacoustics at $\Gamma_2-\Gamma_4$ reorientation in orthoferrites with Kramers rare-earth ions

From the current theory point of view, an analysis of dynamic effects in the neighbourhood of an RPT would logically begin from $TmFeO_3$, a compound with a non-Kramers f ion. In it, since $v_\sigma < v_R$, the soft mode near the $\Gamma_2-\Gamma_4$ transition must be the AFMR σ iron mode, which, in a sense, is the simplest situation possible. In this case the effects of the rare-earth subsystem on the spectrum of coupled vibrations can be safely neglected and we can use the conventional theory [7] for the analysis of experimental data. However, as far as specific calculations are concerned, this theory is known to be oriented on $ErFeO_3$, an orthoferrite with a Kramers rare-earth ion. It should be noted that erbium orthoferrite was not a good choice for checking the theory of Ref. [7]. But it is mainly the unsuccessful attempts to employ this theory for explaining the later data on orthoferrites with Kramers f ions which stimulated its revision. The discussion of experimental data starts with $ErFeO_3$, a material which provides the most interesting and numerous examples of the influence of the rare-earth subsystem on the statics and dynamics of spin reorientation.

2.1.1 $ErFeO_3$. A unique feature of this orthoferrite is that it is one of the few in which, in addition to the ordering of iron near $T \approx 600$ K, a rare-earth ordering at $T \approx 4.1$ K takes place. In this latter process, the paramagnetic to antiferromagnetic transition of erbium [38] is not due to the magnetodipole d – f interaction (which undoubtedly is also present) but rather results from an increase in the f – f exchange with lowering T. As the temperature decreases, by and large three spontaneous second-order RPTs occur in the antiferromagnetic iron structure, two high-temperature transitions ($\Gamma_4-\Gamma_{24}$ at $T_1 \approx 100$ K and $\Gamma_{24}-\Gamma_2$ at $T_2 \approx 90$ K), and one low-temperature transition ($\Gamma_2-\Gamma_{12}$ at $T_3 = T_{N2} \approx 4.1$ K). A special feature of this latter transition is its combined nature in the sense that the ordering of erbium is accompanied by the reorientation of iron in the **bc** plane, meaning that for the rare-earth subsystem this is an ordering (disorder – order) transition, whereas for the iron subsystem this is a typical RPT (order – disorder transition). This feature, as we shall see, plays a central role in determining the dynamics of erbium orthoferrite near T_3.

ME coupled calculations [7] of the AFMR spectra and of the temperature dependence of the sound velocity change near the $ErFeO_3$ $\Gamma_2-\Gamma_4$ transition predict that in the absence of dipole interaction, at second-order RPT points, the velocity of the active shear acoustic mode must vanish and the quasimagnon gap must be ~ 0.1 GHz. In actual fact, however, for all of the REOFs thus far studied, totally different values of at best a few percent for sound velocity change and tens of GHz for frequency gaps has been observed.

The early (Raman scattering) studies [41] of the AFMR spectrum of $ErFeO_3$ revealed a soft σ mode but, as is now evident, yielded a too large gap of ≈ 150 GHz. In addition, the $\Gamma_2-\Gamma_{24}$ and $\Gamma_{24}-\Gamma_4$ transitions were not temperature resolved. Presumably, the reason for all this is the relatively low accuracy of the method. More detailed results on the magnetic vibration spectrum in $ErFeO_3$ were obtained by submillimetre spectroscopy [30, 42]. The theoretical analysis of these data showed that the magnetic resonance at frequencies $\nu \leqslant 3$ cm^{-1} must be due to the soft rare-earth mode. Experiments designed to discover these soft modes in the millimetre wavelength range were undertaken in Refs [15, 18]. The results are given in Fig. 1a. A soft resonance mode of a usual form is seen only in the neighbourhood of the $\Gamma_2-\Gamma_{24}$ transition, the corresponding frequency gap at $T_2 \approx 90$ K being ≈ 25 GHz. At the upper reorientation boundary $T_1 \approx 100$ K, the single wide absorption line over the entire frequency range studied makes it impossible to determine the magnon activation.

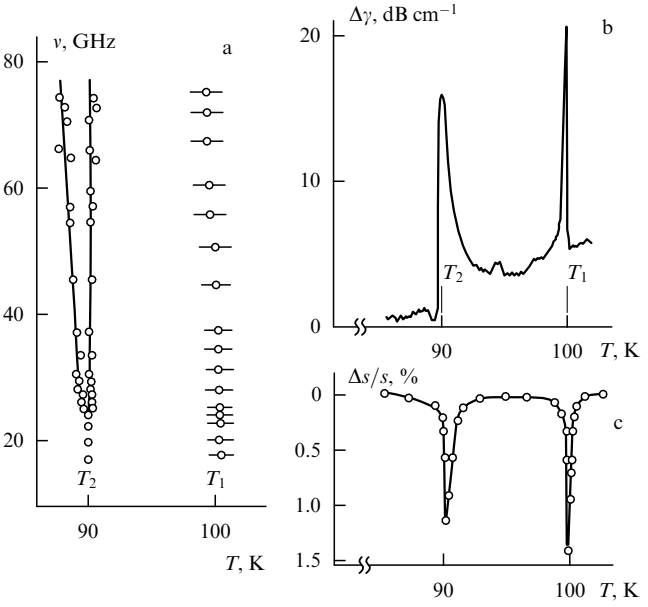

Figure 1. The temperature dependence of the magnetic resonance soft mode frequency (a), the attenuation coefficient change $\Delta\gamma$ (b) and the fractional velocity change $\Delta s/s$ (c) for active transversal sound at the spontaneous reorientation $\Gamma_2-\Gamma_4$ in $ErFeO_3$. T_1 is the $\Gamma_4-\Gamma_{24}$ RPT temperature, T_2 the $\Gamma_{24}-\Gamma_2$ RPT temperature.

The first ultrasonic investigations at the spontaneous reorientation $\Gamma_2-\Gamma_4$ in $ErFeO_3$ were undertaken in Refs [20 – 22]. The maximum decrease in the velocity s of the active shear sound wave at the reorientation boundaries T_1 and T_2 was reported in Ref. [20] and did not exceed 0.3%. Figure 1b show the latest data [15, 18, 19]. It is seen that the anomalies in the relative velocity ($\Delta s/s$) and the attenuation coefficient ($\Delta\gamma$) changes in the active acoustic mode are definitely of a quasiresonant nature and asymmetric with respect to the RPT points T_1 and T_2. Although the relative sound velocity change is nearly an order of magnitude larger than reported previously [20] (most probably due to the

quality of the single crystal used), still it does not exceed 2% and by no means tends to 100%. The change in the attenuation coefficient does not exceed 15 dB cm^{-1}, and the feature at T_2 is broader than that at T_1. In an external magnetic field aligned along the **a** or **c** axes, it is known that only one of RPTs, respectively, either $\Gamma_2-\Gamma_{24}$ or $\Gamma_{24}-\Gamma_4$, must be induced. This is indeed the case experimentally. It should be noted, though, that the acoustic anomalies observed in $ErFeO_3$ in both experimental situations decreased sharply with increasing H [19, 21] and were only seen below $H \leqslant 6$ kOe for $\mathbf{H} \parallel \mathbf{a}$ and below $H \leqslant 3$ kOe for $\mathbf{H} \parallel \mathbf{c}$ (Fig. 2). The absence of a temperature shift contrary to what is expected from the well-known $H-T$ phase diagram is apparently due to errors in measurement geometry.

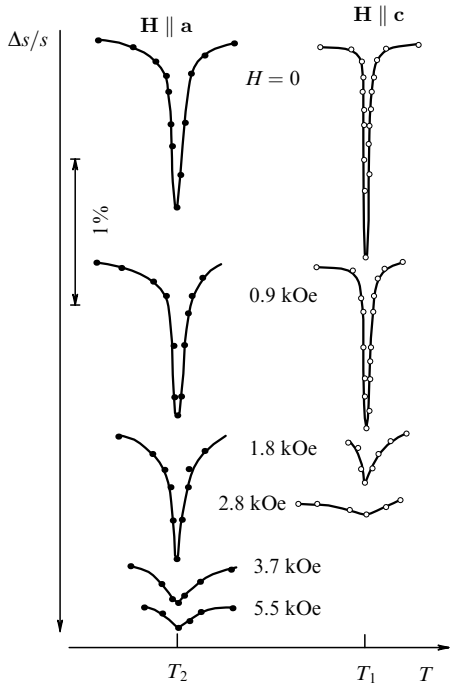

Figure 2. The temperature dependence of the fractional velocity change of the active transversal sound mode $\mathbf{k} \parallel \mathbf{c}$, $\mathbf{u} \parallel \mathbf{a}$ in the RPT region at $T = T_1$, $\mathbf{H} \parallel \mathbf{c}$ and $T = T_2$, $\mathbf{H} \parallel \mathbf{a}$ in $ErFeO_3$. Absorption curves are similar.

2.1.2 $YbFeO_3$. Ytterbium orthoferrite has the lowest-temperature $\Gamma_2-\Gamma_4$ reorientation region [12] among the REOFs studied. A distinguishing feature of the RPT in $YbFeO_3$ is that the polarisation of Yb^{+3} ion magnetic moments in the Γ_2 phase is described not by one but by two irreducible representations, Γ_2 and Γ_8 [43]. The admixture of the Γ_8 phase is due to the significant increase of the f–f interaction, upon cooling. Although this is not seen explicitly in experiment [12], the expectation is that the tendency to the exchange-assisted ordering of the rare-earth ions will make it easier for them to act as an independent system of collective vibrations.

The investigation of the resonant properties of $YbFeO_3$ in the infrared and submillimetre ranges [44] have displayed γ and σ iron AFMR modes and a number of EPR branches, including those due to direct electronic transitions within the basic doublet of the Kramers Yb^{+3} ion. Predictably, the relationship between the frequencies of the f and d subsystems turned out to be such ($\nu_{\gamma,\sigma} > \nu_{R,r}$) that the rare-earth mode must be soft in the RPT region. This mode was not seen in these experiments, however, and as to the σ iron mode, which has the symmetry of a soft mode at the $\Gamma_2-\Gamma_4$ transition, this, bounded as it is by lower-frequency rare-earth modes, was only slightly anomalous in the OPT vicinity. Therefore, when addressing the task of finding a soft resonance mode in the region $\nu < 3$ cm^{-1}, the authors of Ref. [45] were in fact non unaware of its nature. Its rare-earth origin follows from the subsequent calculations of the entire magnetic vibration spectrum of $YbFeO_3$ [30]. The temperature dependence of the resonant frequencies of this mode as measured in Ref. [45] is shown in Fig. 3. Special polarisation measurements carried out in the same study showed absorption lines to be most intensive for $\mathbf{h} \perp \mathbf{F}$, confirming that the mode we are dealing with is the magnetoresonant mode which has the symmetry of a soft mode at the $\Gamma_2-\Gamma_4$ RPT [46]. The above geometry corresponds to the polarisations $\mathbf{h} \parallel \mathbf{c}$ and $\mathbf{h} \parallel \mathbf{a}$ in recording the absorption near the $\Gamma_2-\Gamma_{24}$ and $\Gamma_{24}-\Gamma_4$ transitions. The reason we stress this point is that the absorption near the RPT is not always due to the softening of the magnetic resonance frequency [9, 17]. From the sum total of such records, the temperature dependence of the soft mode frequency shown in Fig. 3 is restored [45]. The temperature boundaries of reorientation, $T_1 = 8.15$ K and $T_2 = 6.85$ K, are determined from the minimum frequency (energy gap) positions found to be $\nu_1 = 20.2$ GHz and $\nu_2 = 37.5$ GHz, respectively. The resonance line widths in the Γ_2 and Γ_4 phases were 5 to 10 GHz. Note that there is a small but perceptible scatter in the absolute values of T_1, T_2, and gaps for samples from various batches of raw material. The scatter may result from differences in the manufacture technology and quality of the single-crystals, from the presence of impurities, and from other, mostly uncontrollable factors, and, to a greater or lesser degree, is characteristic of all REOFs, including

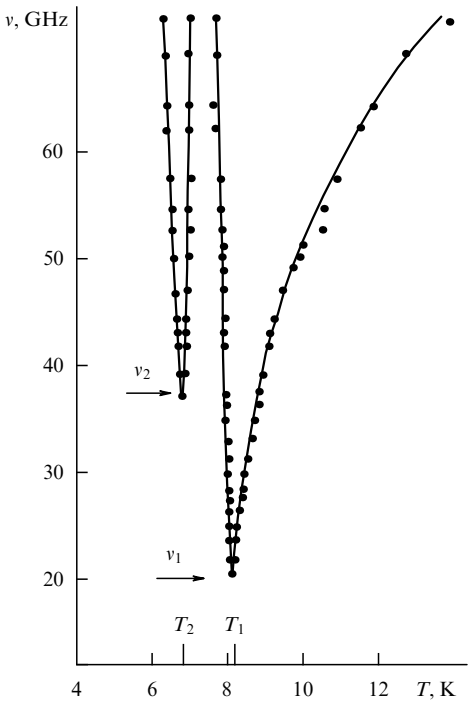

Figure 3. The temperature dependence of the magnetic resonance soft mode frequency at spontaneous reorientation $\Gamma_2-\Gamma_{24}-\Gamma_4$ in $YbFeO_3$ at $\mathbf{h} \parallel \mathbf{c}$ and $\mathbf{h} \parallel \mathbf{a}$ for the $\Gamma_2-\Gamma_{24}$ and $\Gamma_{24}-\Gamma_4$ transitions, respectively.

$YbFeO_3$. Thus, later measurements on $YbFeO_3$ [12] yielded $T_1 = 7.95$ K, $\nu_1 = 21$ GHz, $T_2 = 6.8$ K, $\nu_2 = 38.5$ GHz. We will use these values of the RPT parameters in the following, assuming that the small scatter they show has no basic significance in analyzing the spectra of coupled vibrations. To close this topic, we note that even though defects, inhomogeneities, impurities etc. undoubtedly may cause a gap scatter, a comparison [48] has shown a difference of at most 20% for results obtained on single crystals from various sources.

The above-mentioned sensitivity of the gap values to magnetic field misalignment relative to the **a** and **c** crystal axes is demonstrated in Fig. 4. The $H-T$ phase diagram obtained in Ref. [12] suggests that $\partial T_1/\partial H_a = 0.091$ K kOe^{-1} and $\partial T_2/\partial H_c = -0.092$ K kOe^{-1}, and this is exactly what is seen in the dependences shown in Fig. 4. It will be important to our discussion that for **H** aligned exactly along the axes the value of the gap in $YbFeO_3$ does not depend on the temperature and the transition field (at least up to $H \leqslant 6-7$ kOe).

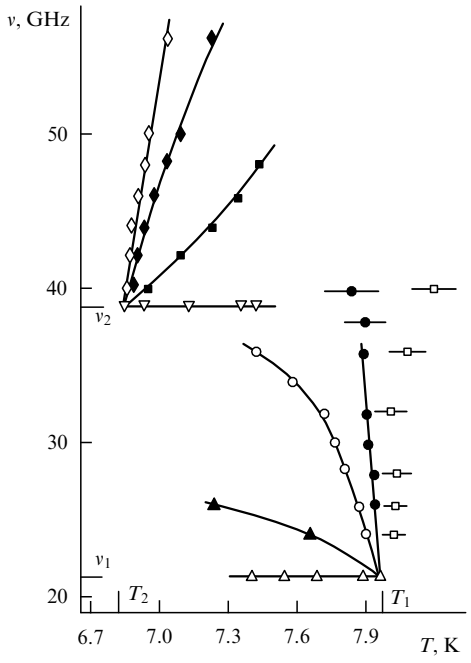

Figure 4. The temperature dependences of the energy gaps in $YbFeO_3$ for induced transitions in the field $\mathbf{H} \parallel \mathbf{a}$ (▽) and $\mathbf{H} \parallel \mathbf{c}$ (△) and for various field misalignments in the **ac** plane. Deviation for the **a** axis: 1° (■), 3° (◆), 5° (◇); deviation from the **c** axis: 1° (▲), 3° (○), 5° (●), 10° (□).

Figure 5 presents the temperature dependence of the relative increment of the sound velocity $\Delta s/s$ and of the sound attenuation $\Delta\gamma$ [12]. In spite of the realisation of the long-wave approximation ($\nu \ll \nu_{me}$) in the experiment, varying the sound frequency in the range 50–250 MHz left $\Delta s/s$ frequency independent even at the RPT points. The effect of the external magnetic field $\mathbf{H} \parallel \mathbf{c}$, on the other hand, is very strong. As anticipated, it shifts the $\Gamma_{24}-\Gamma_4$ transition to lower temperatures but, in contrast to the situation in $ErFeO_3$, enhances acoustic anomalies significantly (Fig. 6). $\Delta s/s$ and $\Delta\gamma$ change in a reversible way nearly linearly with the field, and at $H \approx 35$ kOe become almost an order of magnitude larger than their respective zero-field values. At a more exact alignment of the field along the **c** axis (it was $\approx 0.5°$ in Fig. 6), a further 25% enhancement of the anomalies proved possible. Thus, on the line of the magnetic-field-induced ($\mathbf{H} \parallel \mathbf{c}$) $\Gamma_4-\Gamma_{24}$ transition, at constant magnon gap values (see Fig. 4), a change in the active sound velocity with the field is observed.

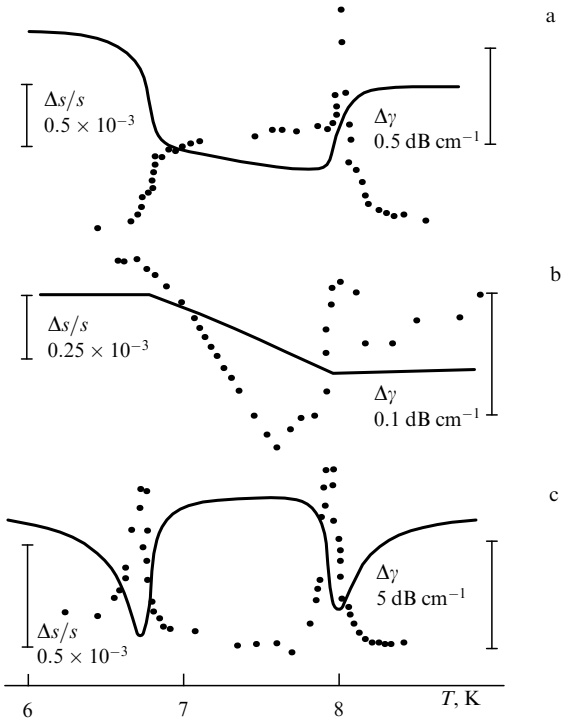

Figure 5. The temperature dependences of the fractional velocity change $\Delta s/s$ (solid lines) and attenuation change $\Delta\gamma$ (dots) of sound with wave vector $\mathbf{k} \parallel \mathbf{c}$ near the $\Gamma_2-\Gamma_4$ reorientation transition in $YbFeO_3$ for various directions of the displacement vector **u**: (a) $\mathbf{u} \parallel \mathbf{c}$; (b) $\mathbf{u} \parallel \mathbf{b}$; (c) $\mathbf{u} \parallel \mathbf{a}$.

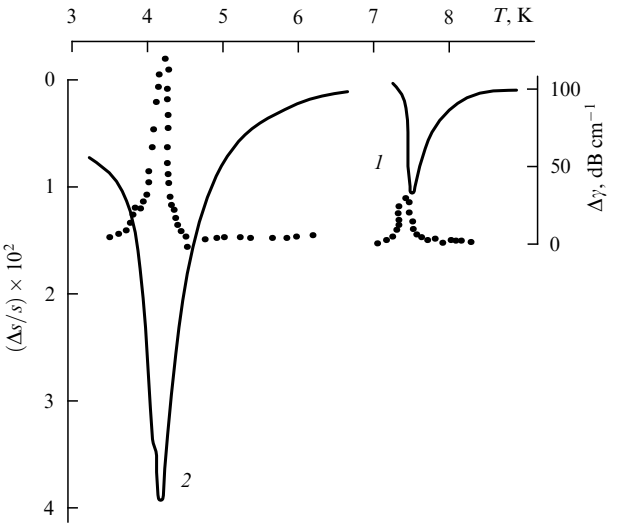

Figure 6. The temperature dependence of the fractional velocity change $\Delta s/s$ (solid line) and the attenuation change $\Delta\gamma$ (dots) of shear sound wave ($\mathbf{k} \parallel \mathbf{c}$, $\mathbf{u} \parallel \mathbf{a}$) in a magnetic field in $YbFeO_3$: *1* — 5 kOe; *2* — 35 kOe.

The following feature which distinguishes $YbFeO_3$ from other REOFs can be noted. When the frequencies of the four vibration subsystems are related by $v_r < v_R < v_\sigma < v_\gamma$, as they do in this orthoferrite, the soft resonance r mode v_r and the soft iron AFMR σ mode v_σ have frequencies which are quite separate from each other. This also takes place — which is precisely the point we wish to make — in the RPT temperature region. In this case — in contrast to, say, $ErFeO_3$ or, as we will see later, to $HoFeO_3$ — the spin dynamics in the reorientation region $\Gamma_2-\Gamma_4$ in the millimetre range is determined virtually completely by the rare-earth ions of the f subsystem. It is therefore the rare-earth type to which the soft resonance mode in $YbFeO_3$ near $v \sim v_{1,2}$ may most justifiably be thought to belong.

2.1.3 $NdFeO_3$. Although no ultrasonic experiments were conducted on this orthoferrite, it is worthwhile to consider the available data on its magnon branch [49] in order to draw some conclusions about the role of the ME coupling . This is the more interesting that the temperature dependence of the magnetic resonance frequencies in $NdFeO_3$ (see Fig. 7) displays a close correlation with that in $ErFeO_3$ (see Fig. 1a). In fact, as in $ErFeO_3$, here too a usual soft mode is observed only at the lower temperature boundary, at the $\Gamma_2-\Gamma_{24}$ transition at point T_2. Two relatively narrow lines ($\delta T \approx 8$ K) get close with decreasing v, merging at $T = T_2 = 92$ K at the energy gap frequency $v_2 = 56$ GHz. At the upper reorientation boundary $T = T_1 = 155$ K, a single line, almost an order of magnitude wider than the absorption lines near T_2, is detected. Therefore the v_1 gap cannot be measured. The experimental points at $T = T_2$ at frequencies $v < v_2$ are related to the absorption from the wings of the resonant lines. The corresponding signals rapidly decrease in amplitude, totally disappearing as the frequency decreases by the linewidth, and are observed in all REOFs on restoring the magnetic resonance frequency – temperature (frequency – field) dependence.

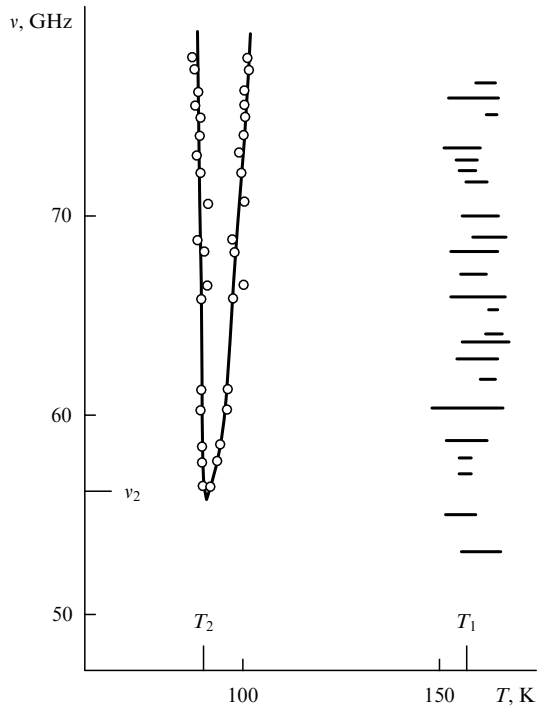

Figure 7. The temperature dependence of the magnetic resonance soft mode at the spontaneous reorientation $\Gamma_2-\Gamma_4$ in $NdFeO_3$.

From neutron spectroscopy data [50], the splitting of the main Kramers ion Nd^{3+} in the Γ_2 phase is $v_R = 120$ GHz, whereas the frequencies of the σ and γ AFMR modes at 300 K are 250 and 500 GHz, respectively [41]. It was therefore reasonable to suggest that the soft resonance mode in $NdFeO_3$ is rare-earth [49]. The above analysis implies, however, that near T_2 the soft mode is the iron one. The boundary temperatures of the $\Gamma_2-\Gamma_4$ reorientation are close to $T_{1,2}$ in $ErFeO_3$ and $TmFeO_3$, but differ significantly in different experiments. This is presumably due to differences in sample quality because single crystals of $NdFeO_3$ show a marked domain growth tendency. This may also account for the wide reorientation region. In this particular experiment its width was about 60 K, whereas in $ErFeO_3$ and $TmFeO_3$, for example, the width $\Delta T = T_1 - T_2 \approx 10$ K. The domain structure of a sample may produce spatial fluctuations in the anisotropy density, very much as in substitutional orthoferrites [51] — the reason why these latter have relatively large ΔT's. The resonance line width δT in $NdFeO_3$ is also four to five times larger than in other orthoferrites, both near T_1 and T_2, suggesting the existence of some correlation between ΔT and δT.

In contrast to $ErFeO_3$, no experimental estimates are available for the parameters of the f – f and d – f interactions in $NdFeO_3$. Nevertheless, the above-mentioned correlation between the experimental data on these orthoferrites (similar temperature dependence of the frequencies, relatively close values of gaps at T_2, and the fact that Nd^{3+} and Er^{3+} are both Kramers ions) suggest that, to a certain extent, the conclusions about the ME coupling in $ErFeO_3$ also hold for $NdFeO_3$. The experimental study of the phonon branch in $NdFeO_3$ is currently being hampered by the lack of high quality single crystals of sufficient size ($L \approx 4-5$ mm) for the conventional ultrasonic technique to work. Because of the domain growth tendency mentioned above, as of now the linear size of the best-quality (domainless) single crystals is $L \approx 1$ mm [49]. Note the technical nature of the limitations impairing the ultrasonic investigation of the ME coupling: physically, even samples this small in size will undoubtedly satisfy the conditions for the existence of an ME gap ($L > s/\omega_{me}$) [6].

2.1.4 $SmFeO_3$. This material has the highest-temperature reorientation interval (≈ 450 – 500 K) among other orthoferrites. Earlier Raman scattering studies [41] of the γ and σ mode spectra yielded, as is now evident, a too large gap of ≃ 150 GHz, the major sources of error being presumably the same as in $ErFeO_3$ measurements. A direct reconstruction of the soft mode spectrum in the millimetre wavelength range [51] led to the following values for the reorientation boundaries and the corresponding gaps: $T_1 = 478$ K, $v_1 = 40$ GHz, $T_2 = 448$ K, $v_2 = 35$ GHz (Fig. 8). Since the absorption lines near the frequency minima proved to be temperature unresolvable because of their low intensity and large width, the energy gaps were obtained, as the figure shows, by extrapolation (to within ±5 GHz). The observed magnetoresonance spectrum is presumably an AFMR σ mode, for the following reasons: (1) the resonance line width is ≈ 15 – 20 GHz, which agrees with other experiments on the σ mode, and (2) there are a close similarity between the observed $v(T)$ dependence and the σ mode spectrum in $TmFeO_3$ (see below), and the sharp difference between the temperature dependence of the

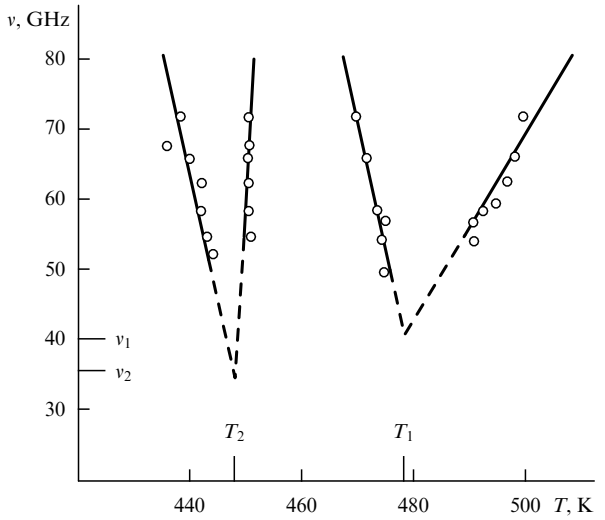

Figure 8. The temperature dependence of the magnetic resonance soft mode at the spontaneous reorientation in $SmFeO_3$.

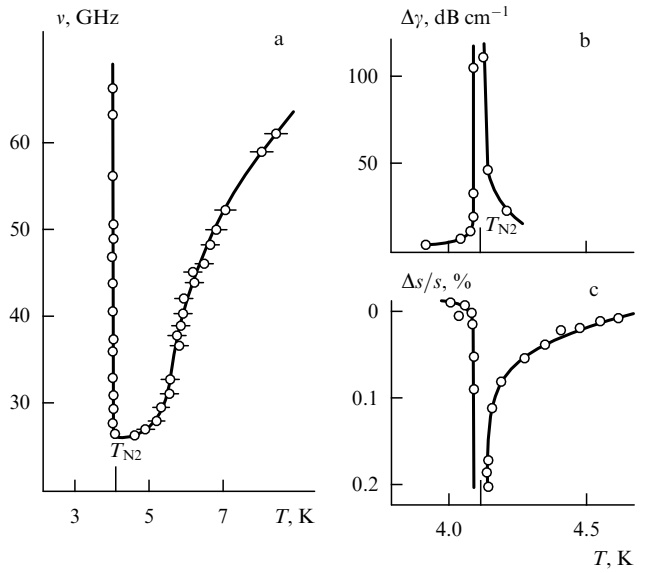

Figure 9. The temperature dependence of the magnetic resonance soft mode (a), attenuation change $\Delta\gamma$ (b), and fractional velocity change $\Delta s/s$ (c) of the active sound ($\mathbf{k} \parallel \mathbf{c}$, $\mathbf{u} \parallel \mathbf{b}$) at spontaneous reorientation $\Gamma_2 - \Gamma_{12}$ in $ErFeO_3$.

$\Gamma_4 - \Gamma_{24}$ soft mode frequencies in $HoFeO_3$ and $ErFeO_3$. Even in $HoFeO_3$, $ErFeO_3$, and $NdFeO_3$, with their much lower values of T_1 and T_2, it proves impossible to find, in the vicinity of T_2, a softening magnetoresonance spectrum in its usual form (as in $YbFeO_3$, for example). Nor can it reasonably be expected in $SmFeO_3$, with presumably even wider rare-earth mode lines.

Note that the absolute gap values obtained here are very close to those in $TmFeO_3$, where the AFMR σ mode is soft.

2.2 Some aspects of magnetoacoustics near the $\Gamma_2 - \Gamma_{12}$ transition in $ErFeO_3$

The low-temperature $\Gamma_2 - \Gamma_{12}$ reorientation in $ErFeO_3$ has been the subject of a probably record number of theoretical and particularly experimental studies. The reason for this is a unique combined nature of this transition (see, e.g., Ref. [52]). The structure of the low-temperature reorientation in $ErFeO_3$ has been thoroughly explored by various experimental techniques including magnetostriction measurements [52], NMR [53, 54], and magnetic susceptibility [56] measurements. This provided the basis for the subsequent dynamical experiments. During the past decade there has been a substantial interest in the high-frequency properties of this transition, such as, e. g., an intermediate state magnetic resonance [57], high-frequency susceptibility [58], dielectric [47] and magnetodynamic [9] resonances, and the temperature and field dependence of the energy gaps [59]. The soft resonance mode, which will concern us in the following, was first discovered in experiments in Ref. [60], however the temperature dependence of its resonance frequencies was reconstructed in detail in Ref. [8].

The results of this experiment are given in Fig. 9a. The spectral features to be recognised here are a pronounced asymmetry with respect to the transition point $T_{N2} = 3.89$ K, and the 'freezing' of the resonance frequencies in an interval ~ 1 K in approaching T_{N2} from the higher temperatures. In elucidating the nature of the soft mode, it is also essential that the slope of the $\nu(T)$ dependence by and large decreases with increasing temperature in the region $T > T_{N2}$.

The value of the transition temperature is determined from the position of the dip in $\nu(T)$ and is in agreement with other independent measurements, in particular with those using the dielectric resonance method [47]. The measured gap ν_{N2} is 26.1 GHz. $ErFeO_3$ samples prepared of different single crystals are found to vary widely in the absolute value of T_{N2} (3.5 – 4.1 K). For example, in ultrasonic studies on $ErFeO_3$ [14, 15], whose results are given below, samples with $T_{N2} = 4.1$ K were used.

As already noted, in a REOF one d and one f mode have a soft mode symmetry. For our further discussion it is essential precisely which of the two actually softens at the transition point. A comparison of the experimental [8, 41] with calculated [46] results led to the conclusion that the soft mode observed is a rare-earth one. This was later confirmed indirectly both experimentally and theoretically [42]. At $T < T_{N2}$ the $\Gamma_2 - \Gamma_{12}$ transition can be induced by the field $\mathbf{H} \parallel \mathbf{a}$. The temperature dependence of the soft mode frequency at induced transitions is presented in Fig. 10 and shows the same features observed for spontaneous reorientation: a sharp asymmetry about the critical field $H = H_a$, and the existence, for $H > H_a$, of a large field interval in which the H dependence of the frequency is anomalously weak (see insert of Fig. 10) and which shrinks with increasing field.

The phonon vibration branch near the low-temperature RPT has been investigated experimentally [14 – 19, 61, 62]. It follows from symmetry arguments that at $T \sim T_{N2}$ the active mode is a shear sound mode with the wave vector $\mathbf{k} \parallel \mathbf{c}$ and polarisation $\mathbf{u} \parallel \mathbf{b}$. As seen in Figs 9b, c, it exhibits giant, resonance-type, highly asymmetric critical anomalies in the sound velocity and attenuation, which have no analogues, either in magnitude or shape, in the neighbourhood of previously found RPTs or ordering transitions in REOFs. The sound wave velocity decrease is accompanied by a sharp increase in attenuation, so much so that at $T \sim T_{N2}$ no signal is detected in experiment. Although this precludes a complete determination of the velocity and attenuation changes at $T = T_{N2}$, even what there is left to measure is an at least 20 – 25% decrease in velocity and a > 100 dB cm^{-1} increase in attenuation.

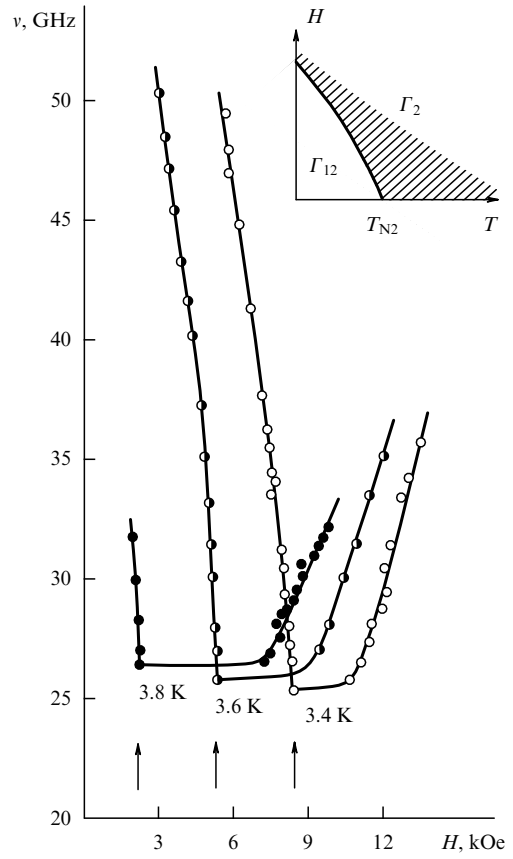

Figure 10. The frequency and field dependences of the soft resonance mode in $ErFeO_3$ in the vicinity of the $\Gamma_2-\Gamma_{12}$ reorientation induced by the field $\mathbf{H} \parallel \mathbf{a}$. Arrows indicate the critical field values H_a at the corresponding temperatures. Insert shows the $T-H$ phase diagram [$H_a(T)$ line of $\Gamma_2-\Gamma_{12}$ second-order transitions]. The dashed line indicates the regions of an anomalously weak temperature and field dependences on the frequency.

From symmetry considerations, the nature of the low-temperature RPT remains unchanged by the application of a magnetic field $\mathbf{H} \parallel \mathbf{a}$, so that this must be a $\Gamma_2-\Gamma_{12}$ transition as before. Indeed, the dependences $\Delta\gamma$ and $\Delta s/s$ for the active mode at $\mathbf{H} \parallel \mathbf{a}$ retain the main features characteristic of a spontaneous transition. Figure 11a shows the magnetic-field dependence of the amplitude A of a sound signal on its passage through a sample for $\mathbf{k} \parallel \mathbf{c}$, $\mathbf{u} \parallel \mathbf{b}$ at various T's. It is seen that, analogous to the spontaneous case, the absorption shows a highly pronounced resonance-type anomaly. With increasing field, its amplitude and width decrease insignificantly. Absorption measurements for the longitudinal acoustic mode (Fig. 11b) and the non-active shear acoustic mode performed near the low-temperature RPT show that anomalies in this latter configuration are markedly smaller (by about two orders of magnitude) than for the active mode. Within the accuracy of the measurement, no sound velocity anomalies were detected in this configuration.

To summarise, then, three aspects of the $\Gamma_2-\Gamma_{12}$ reorientation critical dynamics in $ErFeO_3$ should be noted.

(1) A sharp asymmetry in the $v(T)$, $\Delta s/s(T)$, and $\Delta\gamma(T)$ dependences with respect to the critical temperature T_{N2}. These anomalies, the precursors of the spontaneous transition, occur only in the Γ_2 ($T > T_{N2}$) phase while disappearing abruptly in Γ_{12} ($T < T_{N2}$). Similar $v(H)$, $\Delta s/s(H)$, and $\Delta\gamma(H)$ dependences are seen for a transition induced by a field $\mathbf{H} \parallel \mathbf{a}$.

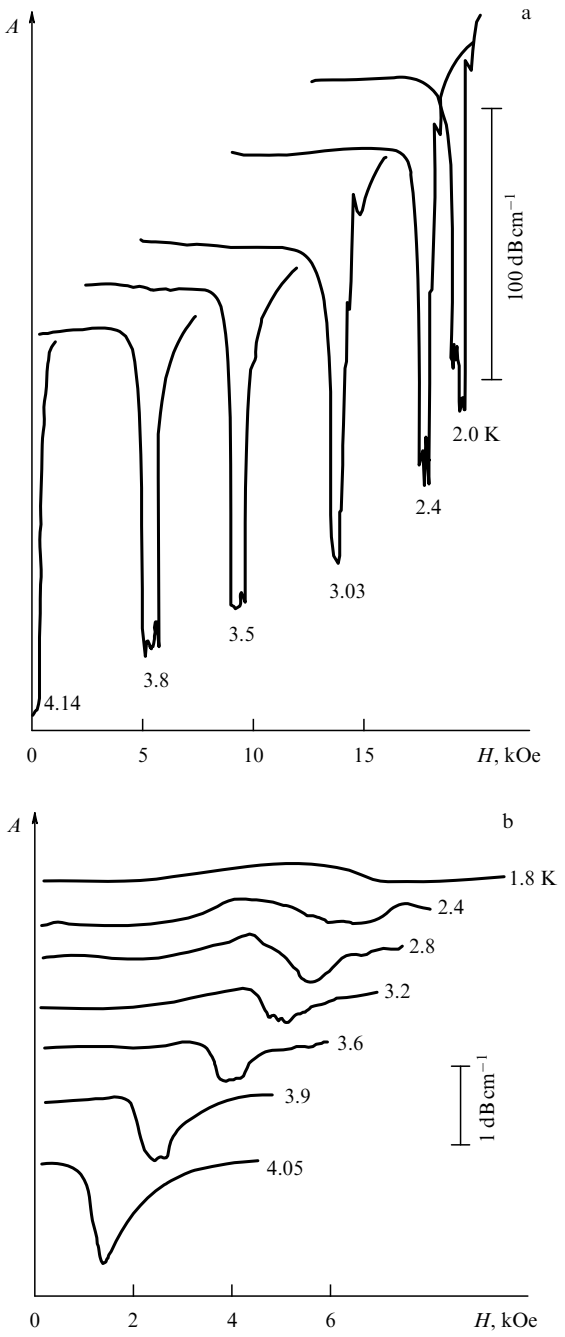

Figure 11. Low-temperature phase transition in $ErFeO_3$: (a) field dependence isothermals of the amplitude A of the active shear sound mode with $\mathbf{k} \parallel \mathbf{c}$, $\mathbf{u} \parallel \mathbf{b}$ after passage through the sample at $\mathbf{H} \parallel \mathbf{a}$, $\nu = 25$ MHz; (b) field dependence isothermals of the acoustic mode for $\mathbf{k} \parallel \mathbf{c}$, $\mathbf{H} \parallel \mathbf{u}$, $\nu = 30$ MHz.

(2) Extremely strong critical sound anomalies. Nothing of the kind has been seen in any other REOF so far (the amplitudes of observed anomalies are typically a few percent at best).

(3) The frequency of the magnetic resonance soft mode in approaching the critical point from $T > T_{N2}$ and $H > H_a$ reaches its minimum long before the critical point and then remains constant all the way to $T = T_{N2}$ or $H = H_a$, respectively. In the same region, the strongest acoustic anomalies are observed.

2.3 Magnetoacoustics at $\Gamma_2-\Gamma_4$ reorientation in orthoferrites with non-Kramers rare-earth ions

2.3.1 $TmFeO_3$. This orthoferrite is, in some sense, antipodal to the ytterbium orthoferrite discussed above. In it, the magnetoresonance branch in the millimetre range can most justifiably be considered as an iron AFMR σ mode. The most convincing evidence for this comes from the study of the full magnetic vibration spectrum in $TmFeO_3$ [63, 64]. But studies of the iron AFMR in this orthoferrite begun earlier in time, when nobody had yet realised the crucial role of rare-earth ions in determining the dynamics of orthoferrites. The spectrum of the soft AFMR mode at a spontaneous transition was calculated [65] (including only the spin-wave system in Fe^{3+}) and a number of experimental studies of the high-frequency properties of this material at induced transitions were conducted (see, e.g., Refs [39, 65, 66]), but this work was rather incomplete and is currently of no significance, especially as far as the problem of the ME coupling is concerned. The experimental gap values, from both resonance [39, 65, 66] and neutron scattering [67] measurements, have a wide scatter and cannot be taken seriously at present. The situation therefore called for new experiments, both to measure the spectrum and to elucidate the nature of the soft magnetoresonance mode. In this connection, let us return to the work of Refs [63, 64], which implies that in the millimetre wave range ($\nu < 3$ cm^{-1}) only one vibration branch, namely the iron AFMR σ mode, can be observed. Its maximum frequency, even away from the transition ($\nu_\sigma \approx 12$ cm^{-1}), is by 5–6 cm^{-1} lower than the lowest direct-transition frequencies within the basic ν_R multiplet in the Tm^{3+} ion; whereas in the reorientation region, where the σ mode is expected to be much weaker than in other orthoferrites, it is subject to a dynamic influence of the f subsystem.

In Ref. [11], the AFMR σ mode was reconstructed by means of a no-field, fixed-frequency, temperature scanning technique. Its temperature dependence is presented in Fig. 12. The energy gaps at the reorientation boundaries $T_1 = 92.5$ K and $T_2 = 81$ K are $\nu_1 = 41$ GHz and $\nu_2 = 40$ GHz, respectively. Line widths in the Γ_2 phase at 40–50 GHz are ≈ 6 GHz.

As in $YbFeO_3$, if aligned strictly enough along the **a** and **c** crystal axes, the magnetic field does not affect the magnitude of the corresponding gaps. For example, in a field $\mathbf{H} \parallel \mathbf{a}$ which induces the $\Gamma_2-\Gamma_{24}$ transition, the gap change $\partial\nu_2/\partial H_a < 0.33$ GHz kOe^{-1} is within the experimental error. The transition temperature grows at a rate of $\partial T_2/\partial H_a = 1.23$ K kOe^{-1}.

The phonon vibration branch in $TmFeO_3$ was investigated in Refs [23] and [24]. We will employ the results of the latter study as more complete and reliable. As before, we will be concerned with the behaviour of the active sound wave with $\mathbf{k} \parallel \mathbf{c}$ and $\mathbf{u} \parallel \mathbf{a}$ near the RPT. The temperature dependence of its velocity and attenuation is shown in Fig. 13. Because sound attenuation becomes strong close to the T_1 and T_2 points, a sound velocity change of only 2–3% was detected in these experiments. We will quote other quantitative results of this study in our general discussion.

2.3.2 $HoFeO_3$. In the orthoferrites considered thus far the spontaneous $\Gamma_2-\Gamma_4$ reorientation occurs via two second-order phase transitions, $\Gamma_4-\Gamma_{24}$ and $\Gamma_{24}-\Gamma_2$. In $HoFeO_3$ this reorientation takes three transitions to occur [68, 69]: $\Gamma_4-\Gamma_{24}$, $\Gamma_{24}-\Gamma_{12}$, and $\Gamma_{12}-\Gamma_2$, at $T_1 = 58$ K, $T_2 = 51$ K,

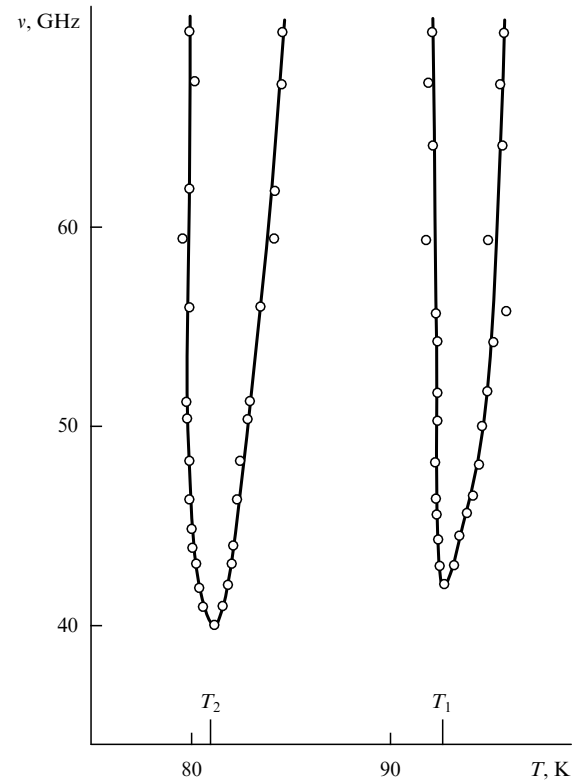

Figure 12. The temperature dependence of the magnetic resonance soft mode at the spontaneous reorientation $\Gamma_2-\Gamma_4$ in $TmFeO_3$.

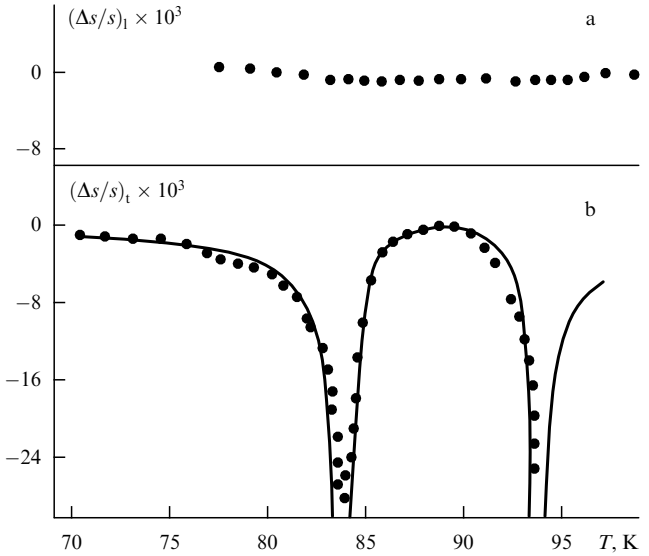

Figure 13. The temperature dependences of the fractional velocity changes of the longitudinal (a) and the active shear (b) sound waves, respectively, with $\mathbf{k} \parallel \mathbf{c} \parallel \mathbf{u}$ and $\mathbf{k} \parallel \mathbf{c}$, $\mathbf{u} \parallel \mathbf{a}$ at the spontaneous $\Gamma_2-\Gamma_4$ reorientation in $TmFeO_3$ (dots show experimental points, line is the theoretical prediction).

and $T_3 = 39$ K, respectively. As the temperature is lowered, at T_1 the vector $\mathbf{G}$ ($\mathbf{F}$) smoothly (as usual) deviates from the **a** (**c**) axis and rotates in the **ac** plane in the interval T_1-T_2. At T_2 the vector $\mathbf{G}$, still 10–20° off the axis, jumps to the **bc** plane, to complete its reorientation by rotating to the **c** axis at T_3. At T_2 the vector $\mathbf{F}$ jumps discontinuously to the **a** axis and has no further visible anomalies. Submillimetre measurements [68, 69] displayed a number of fundamental features

in the dynamics of $HoFeO_3$ near the RPT, notably a strong rare-earth-AFMR mode interaction and a softening of various types of resonance branches. It should be noted that this unusual behaviour of the submillimetre resonance spectrum in this orthoferrite had been reported earlier [70]. Such a complicated dynamics is due to the fact that the rare-earth and AFMR spectra cross repeatedly in the process of reorientation [30]. It was therefore of particular interest to study ME waves under the conditions of a strong interaction between the d and f subsystems.

The SHF and acoustic properties of this orthoferrite were measured in Ref. [13]. Figure 14 presents magnetic resonance results for the millimetre range. From the position of the absorption lines, the phase boundary temperatures were found to be $T_1 = 58$ K, $T_2 = 51.7$ K, and $T_3 = 43$ K. The experimental high-frequency absorption behaviour is consistent with the results of Refs [68, 69], extending them into the lower-frequency region. The two wide absorption maxima near T_1 and T_3 for $\mathbf{h} \parallel \mathbf{a}$ polarisation [13, 37] may be associated with the σ and γ AFMR modes, respectively. Analysis [37, 68, 69] shows the rare-earth and iron modes to be soft near T_1 and T_3, respectively. That the activation of the iron mode at $T = T_3$ was not found in Ref. [13] may be attributed to a strong quasimagnon attenuation due to the influence of the disordered f subsystem [69].

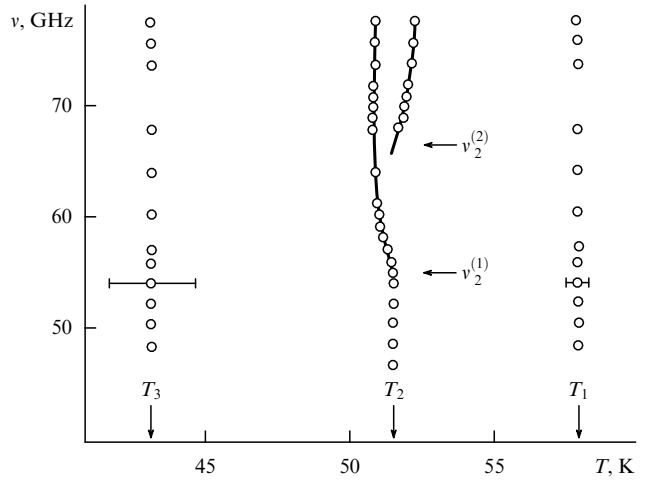

Figure 14. The temperature dependence of the magnetic resonance soft mode at the spontaneous reorientation $\Gamma_2 - \Gamma_{12} - \Gamma_{24} - \Gamma_4$ in $HoFeO_3$.

In the vicinity of T_2, at $\mathbf{h} \parallel \mathbf{c}$ the σ and γ AFMR resonance modes are softened. Absorption lines here are markedly (by about an order of magnitude) narrower than at T_1 and T_3 [13], and at frequencies $\nu > \nu_2^{(2)}$ are well resolvable: during temperature scanning, resonance peaks on either side of the transition point T_2 are seen. The discontinuity in $\nu(T)$, of magnitude $\Delta\nu = \nu_2^{(2)} - \nu_2^{(1)}$, which is observed here is the most convincing proof that at T_2 a second-order phase transition takes place. This is also consistent with the fact that longitudinal sound velocity undergoes a very sharp change compared to what is observed at the T_1 and T_3 points. At the same time, the presence of resonance features in the velocities of various shear waves at T_2 suggests a strong softening of the corresponding magnon modes in the first-order transition $\Gamma_{24} - \Gamma_{12}$ as well. The single lines detected near T_1 and T_3 may result from at least two causes: (1) large energy gaps (> 80 GHz), when the measured absorption is in fact dominated by the wings of the resonance lines, and (2) broad lines and, as a consequence, the merge of two lines into one near T_1 and T_3. All these factors make it impossible to measure the corresponding gaps.

Because of the $\Gamma_2 - \Gamma_4$ reorientation structure described above, the sound waves active at its boundaries are shear ones having different polarisations of the vector $\mathbf{u}$: at T_3, $\mathbf{k} \parallel \mathbf{c}$ and $\mathbf{u} \parallel \mathbf{b}$, and at T_1, $\mathbf{k} \parallel \mathbf{c}$, $\mathbf{u} \parallel \mathbf{a}$ ($\mathbf{k} \parallel \mathbf{a}$, $\mathbf{u} \parallel \mathbf{c}$). The temperature dependence of the corresponding wave velocities displays resonance type features, as expected. One of these is shown in Fig. 15. It is seen that at the $\Gamma_2 - \Gamma_{12}$ transition points the change in the velocity is in excess of 3%. Shown in the same figure is, in particular, the above-mentioned resonance anomaly at the first-order RPT at $T = T_2$. At the high-temperature reorientation boundary T_1 the change in the velocity of active waves ($\mathbf{k} \parallel \mathbf{a}$, $\mathbf{u} \parallel \mathbf{c}$ and $\mathbf{k} \parallel \mathbf{c}$, $\mathbf{u} \parallel \mathbf{a}$) is about two orders of magnitude weaker than at T_3.

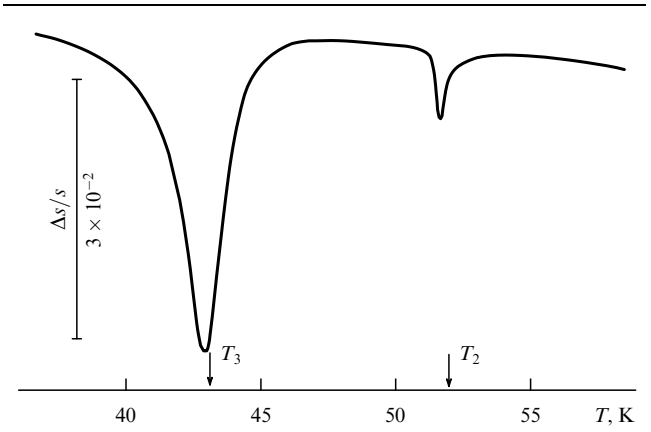

Figure 15. The temperature dependence of the fractional velocity change of the shear sound wave ($\mathbf{k} \parallel \mathbf{c}$, $\mathbf{u} \parallel \mathbf{b}$) at the spontaneous $\Gamma_2 - \Gamma_{12} - \Gamma_{24} - \Gamma_4$ reorientation in $HoFeO_3$.

The magnetic field $\mathbf{H} \parallel \mathbf{a}$ suppresses the Γ_4 phase, so that the corresponding dynamical features disappear during a temperature scanning in a magnetic field. At $H > 1$ kOe, this field also suppresses the complex RPT structure and the associated high-frequency and sound anomalies. Since the gaps at the reorientation boundaries could not be measured for the above reasons, their field dependence remains a moot question unfortunately.

3. Theory of coupled vibrations in rare-earth orthoferrites

The following theoretical results explain most of the current experimental data discussed above.

3.1 Orthoferrites with Kramers rare-earth ions

3.1.1 Orthoferrite energy. We write the free energy density of a REOF in the form [7, 36–38, 69]

$$\mathcal{F} = \mathcal{F}_m + \mathcal{F}_{me} + \mathcal{F}_e \,. \tag{3.1}$$

The energy density of the magnetic subsystem is

$$\mathcal{F}_m = \mathcal{F}_d + \mathcal{F}_{df} + \mathcal{F}_f \,, \tag{3.2}$$

where

$$\mathcal{F}_{\rm d} = \frac{1}{2}\,A\mathbf{F}^2 + \frac{1}{2}\,D(\mathbf{F}\cdot\mathbf{G})^2 - d(F_xG_z - F_zG_x) - 2M_0\mathbf{F}\cdot\mathbf{H} + \frac{1}{2}\,\alpha\left(\frac{\partial\mathbf{G}}{\partial x_i}\right)^2 + \frac{1}{2}\,K^0_{ac}G_z^2 + \frac{1}{2}\,K^0_{ab}G_y^2 + \frac{1}{4}\,K_{20}G_z^4 + \frac{1}{4}\,K'_{20}G_y^4 + \frac{1}{2}\,K''_{20}G_y^2G_z^2\,, \tag{3.2a}$$

$$\mathcal{F}_{\rm df} = -N\Big\{f_x\big[\mu_x(H_x + aF_x) + B'_zG_z\big] + f_y\mu_y(H_y + aF_y) + f_z\big[\mu_z(H_z + aF_z) + B_xG_x\big] + c_x\mu_{xy}(H_y + aF_y) + c_y\big[\mu_{yx}(H_x + aF_x) + B''_zG_z\big] + c_zB_yG_y\Big\}\,, \tag{3.2b}$$

$$\mathcal{F}_{\rm f} = -\frac{1}{2}\,N(\lambda_1f_x^2 + \lambda_2f_y^2 + \lambda_3f_z^2 + \lambda_4c_x^2 + \lambda_5c_y^2 + \lambda_6c_z^2 + 2\lambda_7f_xc_y + 2\lambda_8f_yc_x) - \frac{1}{2}\,NT\big[S(\sigma_1) + S(\sigma_2)\big]\,. \tag{3.2c}$$

Here A, D, α, d, K are the exchange, Dzyaloshinskiĭ, and anisotropy constants in the d subsystem, respectively; $\mathbf{H}$ is the magnetic field; N is the number of ions per cm^3; $\mu_\alpha = \mu_{\alpha\alpha}$, $\mu_{\alpha\beta} = \mu_{\rm B}g_{\alpha\beta}/2$, $\mu_{\rm B}$ is the Bohr magneton, $\hat g$ is the g tensor; a and B are the constants of the isotropic and anisotropic exchange coupling between the d and f subsystems (d–f exchange); λ's are the coupling constants inside the f subsystem; and S is the entropy of the f subsystem,

$$S(\sigma) = \ln 2 - \frac{1}{2}(1+\sigma)\ln(1+\sigma) - \frac{1}{2}(1-\sigma)\ln(1-\sigma)\,,$$
$$\sigma_{1,2} = |\mathbf{f} \pm \mathbf{c}|\,. \tag{3.3}$$

The energy (3.1.2) is written in the two-d two-f sublattice approximation. The vectors $\mathbf{F}$, $\mathbf{G}$, $\mathbf{f}$ and $\mathbf{c}$ have the familiar form

$$\mathbf{F} = \frac{\mathbf{M}_1 + \mathbf{M}_2}{2M_0}\,, \qquad \mathbf{G} = \frac{\mathbf{M}_1 - \mathbf{M}_2}{2M_0}\,,$$
$$\mathbf{f} = \frac{\boldsymbol{\sigma}_1 + \boldsymbol{\sigma}_2}{2}\,, \qquad \mathbf{c} = \frac{\boldsymbol{\sigma}_1 - \boldsymbol{\sigma}_2}{2}\,, \tag{3.4}$$

where the $\mathbf{M}_i$ are the d sublattice magnetisations, $M_0 = |\mathbf{M}_1| = |\mathbf{M}_2| = \mu_{\rm d}N$, $\mu_{\rm d} = 5\mu_{\rm B}$, and $\sigma_{1,2}$ are the mean values of the f ion sublattice Pauli matrices. The sublattices of the d subsystem are considered to be saturated ($D \to \infty$), so that the vectors $\mathbf{F}$ and $\mathbf{G}$ satisfy the additional conditions

$$\mathbf{F}^2 + \mathbf{G}^2 = 1\,, \qquad \mathbf{F}\cdot\mathbf{G} = 0\,. \tag{3.5}$$

The expression for the ME energy will include the d subsystem magnetostriction energy and the interaction energy of the d and f subsystems

$$\mathcal{F}_{\rm me} = \mathcal{F}^{\rm dd}_{\rm me} + \mathcal{F}^{\rm df}_{\rm me}\,, \tag{3.6}$$

where

$$\mathcal{F}^{\rm dd}_{\rm me} = B_{ijkl}G_i\,G_j\,u_{kl}\,, \tag{3.6a}$$
$$\mathcal{F}^{\rm df}_{\rm me} = B^{(1)}_{ijkl}G_if_j\,u_{kl} + B^{(2)}_{ijkl}G_ic_j\,u_{kl}\,, \tag{3.6b}$$

where $\hat u$ is the strain tensor and $\hat B$ is the ME tensor. In the high temperature range ($T \gtrsim 10$ K), because of the f subsystem being in a paramagnetic state there ($f, c \ll 1$), only the first term in (3.6) will be considered. The second term is needed at low temperatures, when the f subsystem is very nearly ordered (for example, at $T \lesssim 4$ K for erbium orthoferrite).

The energy density of the elastic (e) subsystem has the standard form

$$\mathcal{F}_{\rm e} = \frac{1}{2}\,\rho\dot{\mathbf{u}}^2 + c_{ijkl}\,u_{ij}\,u_{kl}\,, \tag{3.7}$$

where $\hat c$ is the tensor of elastic constants, $\mathbf{u}$ is the displacement vector, and ρ is the mass density of the substance. The $\hat B$ and $\hat c$ tensor components will be given in the usual two-index representation in what follows.

3.1.2 Ground state. We consider the case where the reorientation of the vectors $\mathbf{G}$ and $\mathbf{F}$ occurs in the xz plane, and $H = 0$. The equilibrium values of the subsystem parameters in the Γ_2, Γ_4, and Γ_{24} phases are found by minimising the energy (3.1) with respect to $\mathbf{F}$, $\mathbf{G}$, $\mathbf{f}$, $\mathbf{c}$, and u_{ij} under the conditions (3.5), giving

$$F_y = f_y = G_y = c_z = c_x = u^0_{xy} = u^0_{yz} = 0\,,$$
$$F_x = F_0G_z\,, \qquad F_z = -F_0G_x\,, \qquad f_z = \frac{a\mu_zF_z + B_xG_x}{\lambda'_3}\,,$$
$$f_x = \frac{(a\mu_xF_x + B'_zG_z)\lambda'_5 + (a\mu_{yx}F_x + B''_zG_z)\lambda_7}{\lambda'_1\lambda'_5 - \lambda_7^2}\,,$$
$$c_y = \frac{(a\mu_{xy}F_x + B''_zG_z)\lambda'_1 + (a\mu_xF_x + B'_zG_z)\lambda_7}{\lambda'_1\lambda'_5 - \lambda_7^2}\,,$$
$$u^0_{\alpha\alpha} = \frac{\Delta_\alpha}{\Delta}\,, \qquad u^0_{xz} = -\frac{B_{55}G_xG_z}{2c_{55}}\,. \tag{3.8}$$

Here

$$F_0 \approx \frac{1}{A}\left[d + Na(\mu_xf_x + \mu_{yx}c_y)G_z - Na\mu_zf_zG_x\right],$$
$$\lambda'_i = -\lambda_i + \frac{T\operatorname{artanh}\sigma}{\sigma}\,, \qquad \sigma = \sqrt{f_x^2 + f_z^2 + c_y^2}\,, \tag{3.8a}$$
$$\Delta = c_{11}C^2_{2233} + c_{12}C^2_{1323} + c_{13}C^2_{1232}\,,$$
$$\Delta_\alpha = \frac{1}{2}\,E_\alpha C^2_{\beta\beta\gamma\gamma} + E_\beta C^2_{\alpha\gamma\beta\gamma} \qquad (\alpha \neq \beta\,,\ \ \beta \neq \gamma\,,\ \ \alpha \neq \gamma)\,,$$
$$E_\alpha = -2B_{\mu\alpha}G_\mu^2\,, \qquad C^2_{\alpha\beta\gamma\delta} = c_{\alpha\beta}c_{\gamma\delta} - c_{\alpha\gamma}c_{\beta\delta}$$
$$(\alpha, \beta, \gamma, \delta, \mu = 1, 2, 3)\,. \tag{3.8b}$$

Relations (3.8) together with (3.8a) are in fact equations for determining σ, f_x, f_z, and c_y. For $\sigma \ll 1$, they become identities. The components of the antiferromagnetism vector $\mathbf{G}$ of the d subsystem in the collinear Γ_4 phase are $G_x = \pm 1$, $G_z = 0$, and in the collinear Γ_2 phase, $G_x = 0$, $G_z = \pm 1$. Here and throughout this paper, the approximation $\mathbf{G}^2 = 1 - \mathbf{F}^2 \approx 1$ is used. In the angular phase Γ_{24} the equilibrium values of the components of the vector $\mathbf{G}$ are given by the equations

$$G_x^2 = 1 - G_z^2\,, \qquad G_z^2 = -\frac{K_{ac}}{K_2}\,, \tag{3.9}$$

with effective anisotropy constants K_{ac} and K_2 of the form

$$K_{ac} = K^0_{ac} + K^{\rm de}_{ac} + K^{\rm df}_{ac}\,, \tag{3.10}$$

$$K_2 = K_{20} + K^{\rm de}_{20} + K^{\rm df}_{20}\,, \tag{3.11}$$

where the interaction contributions $K_{ac}^{\mathrm{de,df}}$ and $K_{20}^{\mathrm{de,df}}$ are given in the Appendix [Eqns (A.1)]. Note that relations (3.9) in fact also determine G_x and G_z because the λ_i' entering (3.10) [see (A.1)] are dependent on these quantities. For $\sigma \ll 1$ these equations become identities.

Let us formulate the conditions for the stability of the phases under study [7]. Consider the case in which $K_2 > 0$. For $T > T_1$, when $K_{ac} > 0$, the stable phase is Γ_4. As the temperature is lowered, at $T = T_1$ ($K_{ac}(T_1) = 0$) the constant K_{ac} changes sign, the Γ_4 phase loses its stability, and a second-order RPT occurs, the system going over to the angle phase Γ_{24} in which the orientation of the vector $\mathbf{G}$ is determined by (3.9). The reorientation process ends with another second-order RPT at $T = T_2$ ($K_{ac}(T_2) + K_2(T_2) = 0$), at which the system becomes Γ_2. In erbium orthoferrite, also a second-order $\Gamma_2 - \Gamma_{12}$ RPT occurs [14, 15, 61]. This happens at $T = T_3 = T_{\mathrm{N2}} = 4.11$ K, when $K_{cb}(T_3) = 0$, where

$$K_{cb} = K_{ab}^0 + K_{20}'' - K_{ac}^0 - K_{20} + K_{cb}^{\mathrm{de}} + K_{cb}^{\mathrm{df}} . \tag{3.12}$$

The constants $K_{cb}^{\mathrm{de,df}}$ are given in (A.1).

Note that equations (3.9)–(3.12) are written in the K, B, $d \ll A$, $a = 0$ approximation.

3.1.3 Equations of motion. The starting point for the discussion of the f subsystem dynamics are the Landau–Lifshitz-type equations

$$M_{\mathrm{B}} \frac{\dot{\mathbf{f}}}{g} = -\mathbf{f} \times \vec{\mathcal{F}}_f - \mathbf{c} \times \vec{\mathcal{F}}_c + M_{\mathrm{B}} \frac{\mathbf{R}_f}{g} ,$$
$$M_{\mathrm{B}} \frac{\dot{\mathbf{c}}}{g} = -\mathbf{f} \times \vec{\mathcal{F}}_c - \mathbf{c} \times \vec{\mathcal{F}}_f + M_{\mathrm{B}} \frac{\mathbf{R}_c}{g} , \tag{3.13}$$

whose validity for this subsystem is justified in Refs [37, 69], and where $g = 2\mu_{\mathrm{B}}$, $M_{\mathrm{B}} = \mu_{\mathrm{B}} N$, $\vec{\mathcal{F}}_f = \partial\mathcal{F}/\partial\mathbf{f}$, $\mathbf{R}$'s are the relaxational terms given by Ref. [7]

$$\mathbf{R}_f = \Lambda_{\mathrm{f}}\{\mathbf{f} \times \dot{\mathbf{f}} + \mathbf{c} \times \dot{\mathbf{c}}\} , \qquad \mathbf{R}_c = \Lambda_{\mathrm{f}}\{\mathbf{f} \times \dot{\mathbf{c}} + \mathbf{c} \times \dot{\mathbf{f}}\} , \tag{3.14}$$

and Λ_{f} is the dissipation constant in the f subsystem. Note that taking the relaxational term in the form of (3.14) allows the vectors $\mathbf{f}$ and $\mathbf{c}$ to be subject to the additional conditions

$$\mathbf{f}^2 + \mathbf{c}^2 = 1 , \qquad \mathbf{f} \cdot \mathbf{c} = 0 \tag{3.15}$$

analogous to conditions (3.5) for the $\mathbf{F}$ and $\mathbf{G}$ vectors. Relations (3.5) and (3.15) exclude automatically the longitudinal vibrations of the d and f systems.

The dynamics of the d subsystem are described by Eqns (3.13)–(3.15) in which M_{B} is replaced by M_0, $\mathbf{f}$ by $\mathbf{F}$, $\mathbf{c}$ by $\mathbf{G}$, and Λ_{f} by Λ_{d}, where Λ_{d} is the d subsystem dissipation parameter; also, the terms on the right-hand side of Eqns (3.13) must have their signs changed.

The dynamical properties of the elastic subsystem will be analysed in a standard way by means of the equations of motions in terms of displacements

$$\rho \ddot{u}_i = \frac{\partial \sigma_{ik}}{\partial x_k} , \tag{3.16}$$

where $\sigma_{ik} = \partial\mathcal{F}/\partial u_{ik}$ is the elastic stress tensor. The dissipation in the elastic subsystem is neglected as small.

If there are electromagnetically excited spin and elastic waves in the system, the set of equations (3.13)–(3.16) must be complemented by Maxwell's equations

$$\operatorname{curl} \mathbf{E} = -\frac{1}{v} \frac{\partial}{\partial t}(\mathbf{H} + 4\pi\mathbf{M}) , \qquad \operatorname{curl} \mathbf{H} = \frac{1}{v} \varepsilon \frac{\partial \mathbf{E}}{\partial t} ,$$
$$\operatorname{div}(\mathbf{H} + 4\pi\mathbf{M}) = 0 , \qquad \operatorname{div} \mathbf{E} = 0 . \tag{3.17}$$

Here $\mathbf{E}$ and $\mathbf{H}$ are, respectively, the electric and magnetic field strengths, v is the velocity of light in vacuum, ε is the dielectric permittivity of the REOF (it being assumed that at the frequencies of interest the dielectric permittivity tensor is $\varepsilon_{ik} = \varepsilon\delta_{ik}$ and the electrical conductivity vanishes), and $\mathbf{M}$ is the net magnetisation of the REOF:

$$\mathbf{M} = \mathbf{M}_{\mathrm{d}} + \mathbf{M}_{\mathrm{f}} , \qquad \mathbf{M}_{\mathrm{d}} = 2M_0\mathbf{F} ,$$
$$\mathbf{M}_{\mathrm{f}} = N(\mu_x f_x + \mu_{yx} c_y ,\ \mu_y f_y + \mu_{xy} c_x ,\ \mu_z f_z) . \tag{3.18}$$

The above equations describe completely the coupled vibrations of the rare-earth, ferrous, elastic, and dipole subsystems in a REOF.

3.1.4 Dispersion equations and vibration spectra. To obtain dispersion equations involves linearisation of the equations of motion of Section 3.1.3 near the equilibrium position (3.8). Depending on the magnetic phase considered, the dispersion equations for z-propagating harmonic waves take the following form.

(1) Phase Γ_4. Symmetry modes Γ_{23}:

$$(\omega^2 - \omega_{5k}^2)(\omega^2 - \tilde{\omega}_{2k}^2)(\omega^2 - \tilde{\omega}_{1\mathrm{f}}^2)(\omega^2 - \tilde{\omega}_{2\mathrm{f}}^2)$$
$$- \tilde{\omega}_{\mathrm{E}}\omega_{\mathrm{me}5}\omega_{5k}^2(\omega^2 - \tilde{\omega}_{1\mathrm{f}}^2)(\omega^2 - \tilde{\omega}_{2\mathrm{f}}^2)$$
$$- \omega^2\tilde{\omega}_{\mathrm{E}}\tilde{\omega}_{1\mathrm{df}}^3(\omega^2 - \omega_{5k}^2) + \tilde{\omega}_{\mathrm{E}}\tilde{\omega}_{2\mathrm{df}}\tilde{\omega}_{1\mathrm{f}}^2(\omega^2 - \omega_{5k}^2)\tilde{\omega}_{2\mathrm{f}}^2 = 0 . \tag{3.19}$$

The characteristic frequencies entering this equations are given in the Appendix [Eqns (A.2)].

Here and in what follows we use the approximation in which the constant A dominates all the other constants in (3.1), i.e., ω_{E} is much larger than all the other frequencies entering coupled vibration dispersion equations. Also, we restrict ourselves to the case $a = 0$, because the terms in a occur with a small factor F_0 in the equations of interest.

Let us present the solution of (3.19) for the quasispin and quasiacoustic branches in the region of small wave numbers k (long wavelength approximation), vk/ε, $\omega_{5k} \ll \omega_{20,\,1\mathrm{f},\,2\mathrm{f}}$. Assume for simplicity that $\tilde{\lambda}_7 = \tilde{\lambda}_8 = B_z' = 0$. Then one of the rare-earth modes ($\omega_{1\mathrm{f}}$) is uncoupled from the d and elastic modes:

$$\omega_{\mathrm{I}}^2 = \begin{cases} \tilde{\omega}_{2k}^2 + \tilde{\omega}_{2\mathrm{f}}^2\tilde{\zeta}_{\mathrm{df}} + \omega_{5k}^2\tilde{\zeta}_{5k} , & \tilde{\omega}_{2k} > \tilde{\omega}_{2\mathrm{f}} , \\ \tilde{\omega}_{2k}^2(1 - \tilde{\zeta}_{\mathrm{df}}) + \omega_{5k}^2\tilde{\zeta}_{5k} , & \tilde{\omega}_{2k} < \tilde{\omega}_{2\mathrm{f}} , \end{cases}$$

$$\omega_{\mathrm{II}}^2 = \begin{cases} \tilde{\omega}_{2\mathrm{f}}^2(1 - \tilde{\zeta}_{\mathrm{df}}) , & \tilde{\omega}_{2k} > \tilde{\omega}_{2\mathrm{f}} , \\ \tilde{\omega}_{2\mathrm{f}}^2 + \tilde{\omega}_{2k}^2\tilde{\zeta}_{\mathrm{df}} , & \tilde{\omega}_{2k} < \tilde{\omega}_{2\mathrm{f}} , \end{cases}$$

$$\omega_{\mathrm{III}}^2 = \frac{\omega_{5k}^2(1 - \tilde{\zeta}_{\mathrm{df}} - \tilde{\zeta}_{5k})}{1 - \tilde{\zeta}_{\mathrm{df}}} , \tag{3.20}$$

where

$$\tilde{\zeta}_{\mathrm{df},\,5k} = \frac{\tilde{\omega}_{\mathrm{E}}\tilde{\omega}_{2\mathrm{df},\,\mathrm{me}5}}{\tilde{\omega}_{2k}^2} . \tag{3.21}$$

Note that, from here on, the factor $r = (1 - v^2k^2/\varepsilon\omega^2)^{-1}$ in (A.2) should be set equal to unity and zero, respectively, in writing the frequencies of the quasispin branches $\omega_{\mathrm{I,II}}$ and of the quasielastic branch ω_{III}.

(2) Phase Γ_2. Symmetry modes Γ_{12} (a) and Γ_{34} (b):

$$(\omega^2 - \omega^2_{4k,\,5k})(\omega^2 - \tilde{\omega}^2_{1k,\,2k})(\omega^2 - \tilde{\omega}^2_{1\mathrm{f},\,2\mathrm{f}}) - \tilde{\omega}_{\mathrm{E}}\omega_{\mathrm{me4,\,me5}}\omega^2_{4k,\,5k}(\omega^2 - \tilde{\omega}^2_{1\mathrm{f},\,2\mathrm{f}}) - \tilde{\omega}_{\mathrm{E}}\tilde{\omega}_{1\mathrm{df},\,2\mathrm{df}}\tilde{\omega}^2_{1\mathrm{f},\,2\mathrm{f}}(\omega^2 - \omega^2_{4k,\,5k}) = 0\,. \qquad (3.22\mathrm{a,b})$$

The characteristic frequencies in these equations are given by (A.3).

The long wavelength solution of the dispersion equations (3.22) for the quasispin and quasiacoustic branches is determined by (3.20) and (3.21), for which indices 2 and 5 in Eqns (3.22a) should be replaced by 1 and 4, respectively.

3.2 Orthoferrites with non-Kramers rare-earth ions

3.2.1 Ground state. REOFs with non-Kramers f ions include, for example, the thulium and holmium orthoferrites $TmFeO_3$ and $HoFeO_3$ discussed above.

The free energy density of a REOF with non-Kramers f ions is determined by Eqns (3.1)–(3.5). The energy density of the d subsystem is, as before, given by (3.2a), whereas for the interaction energy of the f and d subsystems and for the energy of the f subsystem, instead of (3.2b) and (3.2c), the formulas [36]

$$\mathcal{F}_{\mathrm{df}} = -N\left[\mu_x(H_x + aF_x)f_\xi + BG_z f_\xi + \mu_y(H_y + aF_y)c_\xi\right], \qquad (3.23)$$

$$\mathcal{F}_{\mathrm{f}} = -N\left\{\frac{1}{2}\,\lambda_{\mathrm{f}} f_\xi^2 + \frac{1}{2}\,\lambda_c c_\xi^2 + \frac{1}{2}\,T\left[S(\sigma_1) + S(\sigma_2)\right] + \Delta_{\mathrm{CF}} f_\xi\right\} \qquad (3.24)$$

should be used. Here ξ, η and ζ axes refer to a local coordinate system associated with the f ion sublattices, and Δ_{CF} is the splitting of the f ions quasidoublet in the crystal field.

We assume again that the reorientation of **G** and **F** occurs in the xz plane and that $H = 0$. The equilibrium parameters of all the subsystems in the Γ_2, Γ_4, and Γ_{24} phases are

$$f_\eta = F_y = \mathbf{c} = u^0_{xy} = u^0_{yz} = 0\,,$$

$$f_\xi = f_0 \sin\psi \equiv \frac{\Delta^0_{\mathrm{ex}} G_z}{\tilde{T} - \lambda'_{\mathrm{f}}}\,, \qquad f_\zeta = f_0\cos\psi\,,$$

$$F_x = F_0 G_z\,, \qquad F_z = -F_0 G_x\,,$$

$$u^0_{\alpha\alpha} = \frac{\Delta_\alpha}{\Delta}\,, \qquad u^0_{xz} = -\frac{B_{55}G_xG_z}{2c_{55}}\,, \qquad (3.25)$$

where

$$F_0 = \frac{d + Na\mu_x f_\xi G_z}{A}\,, \qquad \tilde{T} = \frac{\Delta_{\mathrm{f}}}{f_0}\,, \qquad f_0 = \tanh\left(\frac{\Delta_{\mathrm{f}}}{T}\right),$$

$$\sin\psi = \frac{\Delta_{\mathrm{ex}}}{\Delta_{\mathrm{f}}}\,, \qquad \cos\psi = \frac{\Delta_{\mathrm{CF}}}{\Delta_{\mathrm{f}}}\,, \qquad \Delta^2_{\mathrm{f}} = \Delta^2_{\mathrm{CF}} + \Delta^2_{\mathrm{ex}}\,,$$

$$\Delta_{\mathrm{ex}} = \Delta^0_{\mathrm{ex}} G_z + \lambda'_{\mathrm{f}} f_\xi\,, \qquad \Delta^0_{\mathrm{ex}} = B + \frac{\mu_x a d}{A}\,,$$

$$\lambda'_{\mathrm{f}} = \lambda_{\mathrm{f}} + \Delta\lambda_{\mathrm{f}} G_z^2\,, \qquad \Delta\lambda_{\mathrm{f}} = \frac{N(a\mu_x)^2}{A}\,. \qquad (3.26)$$

The remaining notation is as in Section 3.1.

In the angular phase Γ_{24}, the equilibrium components of the antiferromagnetism vector **G** of the d subsystem are as before given by Eqns (3.9)–(3.11), in which

$$K^{\mathrm{df}}_{ac} = -\frac{N\Delta^{02}_{\mathrm{ex}}}{\tilde{T} - \lambda'_{\mathrm{f}}}\,, \qquad K^{\mathrm{df}}_{20} = -\frac{N\Delta\lambda_{\mathrm{f}}\Delta^{02}_{\mathrm{ex}}}{(\tilde{T} - \lambda'_{\mathrm{f}})^2}\,. \qquad (3.27)$$

The phase stability conditions and the conditions on the RPT points $\Gamma_4 - \Gamma_{24}$ and $\Gamma_2 - \Gamma_{24}$ remain the same as for REOFs with Kramers f ions. Conditions for the occurrence of one further phase transition of interest, $\Gamma_2 - \Gamma_{12}$, will be given below.

3.2.2 Dispersion equations and vibration spectra. The dispersion of the coupled vibrations of the f, d, and electromagnetic subsystems in REOFs with non-Kramers f ions will be obtained using the set of initial equations of motion (3.13)–(3.18). In the last of these, the contribution of the f ions to the net magnetisation should be taken in the form

$$\mathbf{M}_{\mathrm{f}} = N(\mu_x f_\xi, \mu_y c_\xi, 0)\,. \qquad (3.28)$$

Upon linearisation of the set of equations (3.13)–(3.18) near the equilibrium position (3.25), depending on the magnetic phase under consideration the dispersion equation for a z-propagating wave takes the following form.

(1) Phase Γ_{24}:

$$\left[(\omega^2 - \omega^2_{4k})(\omega^2 - \tilde{\omega}^2_{2k}) - \tilde{\omega}_{\mathrm{E}}\omega_{\mathrm{me4}}\omega^2_{4k}G_z^2\right]\left\{(\omega^2 - \omega^2_{3k}) \times (\omega^2 - \omega^2_{5k})\left[(\omega^2 - \tilde{\omega}^2_{1\mathrm{f}})(\omega^2 - \tilde{\omega}^2_{1k}) - \tilde{\omega}_{\mathrm{E}}\tilde{\omega}_{\mathrm{f}}\omega_{\mathrm{ex}}\omega'_{\mathrm{ex}}G_x^2\right] - \tilde{\omega}_{\mathrm{E}}\omega^2_{5k}\omega_{\mathrm{me5}}(G_z^2 - G_x^2)^2(\omega^2 - \omega^2_{3k})(\omega^2 - \tilde{\omega}^2_{1\mathrm{f}}) - \tilde{\omega}_{\mathrm{E}}\omega^2_{3k}\omega_{\mathrm{me3}}G_x^2G_z^2(\omega^2 - \omega^2_{5k})(\omega^2 - \tilde{\omega}^2_{1\mathrm{f}})\right\} = 0\,. \qquad (3.29)$$

The parameters in this equations are defined in the Appendix [Eqn (A.4)].

The long wavelength solution of the dispersion equation (3.29) vk/ε, $\omega_{ik} \ll \omega_{1\mathrm{f},\,10,\,20}$ $(i = 3, 4, 5)$ is

$$\omega^2_{\mathrm{I}} = \begin{cases} \tilde{\omega}^2_{1k} + \tilde{\omega}^2_{1\mathrm{f}}\tilde{\zeta}_{\mathrm{df}} + \omega^2_{5k}\tilde{\zeta}_{5k} + \omega^2_{3k}\tilde{\zeta}_{3k}\,, & \tilde{\omega}_{1k} > \tilde{\omega}_{1\mathrm{f}}\,, \\ \tilde{\omega}^2_{1k}(1 - \tilde{\zeta}_{\mathrm{df}}) + \omega^2_{5k}\tilde{\zeta}_{5k} + \omega^2_{3k}\tilde{\zeta}_{3k}\,, & \tilde{\omega}_{1k} < \tilde{\omega}_{1\mathrm{f}}\,, \end{cases}$$

$$\omega^2_{\mathrm{II}} = \begin{cases} \tilde{\omega}^2_{1\mathrm{f}}(1 - \tilde{\zeta}_{\mathrm{df}})\,, & \tilde{\omega}_{1k} > \tilde{\omega}_{1\mathrm{f}}\,, \\ \tilde{\omega}^2_{1\mathrm{f}} + \tilde{\omega}^2_{1k}\tilde{\zeta}_{\mathrm{df}}\,, & \tilde{\omega}_{1k} < \tilde{\omega}_{1\mathrm{f}}\,, \end{cases}$$

$$\omega^2_{\mathrm{III}} = \tilde{\omega}^2_{2k} + \omega^2_{4k}\tilde{\zeta}_{4k}\,, \qquad \omega^2_{\mathrm{IV}} = \omega^2_{4k}(1 - \tilde{\zeta}_{4k})\,,$$

$$\omega^2_{\mathrm{V,\,VI}} = \frac{1}{2(1 - \tilde{\zeta}_{\mathrm{df}})}\left\{\omega^2_{3k}(1 - \tilde{\zeta}_{3k} - \tilde{\zeta}_{\mathrm{df}}) + \omega^2_{5k}(1 - \tilde{\zeta}_{5k} - \tilde{\zeta}_{\mathrm{df}}) \pm \left[\left(\omega^2_{3k}(1 - \tilde{\zeta}_{3k} - \tilde{\zeta}_{\mathrm{df}}) - \omega^2_{5k}(1 - \tilde{\zeta}_{5k} - \tilde{\zeta}_{\mathrm{df}})\right)^2 + 4\omega^2_{5k}\omega^2_{3k}\tilde{\zeta}_{3k}\tilde{\zeta}_{5k}\right]^{1/2}\right\}, \qquad (3.30)$$

where

$$\tilde{\zeta}_{\mathrm{df}} = \frac{\tilde{\omega}_{\mathrm{E}}\tilde{\omega}_{1\mathrm{df}}G_x^2}{\tilde{\omega}^2_{1k}}\,, \qquad \tilde{\zeta}_{3k} = \frac{\tilde{\omega}_{\mathrm{E}}\omega_{\mathrm{me3}}G_z^2G_x^2}{\tilde{\omega}^2_{1k}}\,,$$

$$\tilde{\zeta}_{4k} = \frac{\tilde{\omega}_{\mathrm{E}}\tilde{\omega}_{\mathrm{me4}}G_z^2}{\tilde{\omega}^2_{2k}}\,, \qquad \tilde{\zeta}_{5k} = \frac{\tilde{\omega}_{\mathrm{E}}\omega_{\mathrm{me5}}(G_z^2 - G_x^2)^2}{\tilde{\omega}^2_{1k}}\,. \qquad (3.31)$$

(2) Phase Γ_4:

All results for Γ_4 are obtained from (3.29)–(3.31) by setting $G_x = 1$, $G_z = 0$, $\cos\psi = 1$.

(3) Phase Γ_2:

$$\Big\{\big[(\omega^2-\tilde\omega^2_{1k,2k})(\omega^2-\tilde\omega^2_{1f,2f})-\tilde\omega_f\,\tilde\omega_{cb,ca}\omega_{ax,ay}\omega'_{ax,ay}\big]\times(\omega^2-\omega^2_{4k,5k})-\omega^2_{4k,5k}\omega_{me4,me5}\big[\tilde\omega_E(\omega^2-\tilde\omega^2_{1f,2f})+\tilde\omega_f\,\omega_{ax,ay}\omega'_{ax,ay}\big]\Big\}(\omega^2-\omega^2_{3k})=0\,. \tag{3.32}$$

The characteristic vibration frequencies are determined by Eqns (A.5).

Note that the Γ_2 phase is stable for $K_{cb}>0$ and $K_2+K_{ac}<0$. At temperature $T=T_3$ $(K_{cb}(T_3)=0)$ this phase undergoes a second-order RPT to the angle phase Γ_{12}, and at $T=T_2$ $(K_2(T_2)+K_{ac}(T_2)=0)$, to the angle phase Γ_{24}.

The solution of the dispersion equation (3.32) in the long wavelength limit $\omega_{4k,5k}\ll\omega_{1f,2f,10,20}$ is

$$\omega_I^2=\begin{cases}\tilde\omega^2_{2k}+\tilde\omega^2_{2df}+\omega^2_{5k}\tilde\zeta_{5k}\,, & \tilde\omega_{2k}>\tilde\omega_{2f}\,,\\ \tilde\omega^2_{2k}-\dfrac{\tilde\omega^2_{2df}\tilde\omega^2_{2k}}{\tilde\omega^2_{2f}}+\omega^2_{5k}\tilde\zeta_{5k}\,, & \tilde\omega_{2k}<\tilde\omega_{2f}\,,\end{cases}$$

$$\omega_{II}^2=\begin{cases}\tilde\omega^2_{2f}-\tilde\omega^2_{2df}\,, & \tilde\omega_{2k}>\tilde\omega_{2f}\,,\\ \tilde\omega^2_{2f}+\dfrac{\tilde\omega^2_{2df}\tilde\omega^2_{2k}}{\tilde\omega^2_{2f}}\,, & \tilde\omega_{2k}<\tilde\omega_{2f}\,,\end{cases}$$

$$\omega^2_{III}=\omega^2_{5k}(1-\tilde\zeta_{5k})\,, \tag{3.33}$$

where

$$\tilde\omega^2_{2df}=\frac{\omega_{ay}\omega'_{ay}\tilde\omega_f}{\tilde\omega_E}\,,\qquad \tilde\zeta_{5k}=\frac{\tilde\omega_E\omega_{me5}}{\tilde\omega^2_{2k}}\,. \tag{3.34}$$

The remaining three frequencies $(\omega_{IV}-\omega_{VI})$ are expressed by formulas (3.33) except for the index replacements I–III $\to$ IV–VI, $2,5\to1,4$ and $y\to x$.

4. Discussion of results

Thus, the proposed approach to the dynamics of orthoferrites relies on the theoretically achievable simultaneous solution of the linearised Landau–Lifshitz, Maxwell, and elasticity equations. For each phase of interest (Γ_2, Γ_4, Γ_{24}, Γ_{12}, etc.), one can solve the dispersion equation for the real modes existing in the magnetic material, and thus to describe the experimentally observed diversity in the behaviour of both soft magnon and acoustic modes. With this recognition, we must conclude that the question is in principle quite clear, and that the following factors determine all the diversity of the ways in which RPTs manifest themselves in various orthoferrites: (i) the unusual frequency behaviour of the quasiferromagnetic, rare-earth, and elastic subsystems; the magnetoelastic and f–d coupling parameters; the attenuation parameters of the d and f subsystems; the behaviour of anisotropy constants, etc., and (ii) various types of real experimental limitations, such as (structural, temperature, or magnetic) inhomogeneities in single crystals used; nonzero frequencies really employed; insufficient sensitivity or resolving power of the apparatus (in frequency, field, temperature), etc. Unfortunately, neither group of factors is known to any sufficient degree, which causes large uncertainties in the interpretation of experimental data.

With this understanding, let us analyse the results of the experiments described in Section 2.

4.1 Coupled vibrations in rare-earth orthoferrites with Kramers rare-earth ions near phase transitions

4.1.1 $\Gamma_4-\Gamma_{24}$ transition in $ErFeO_3$ and $YbFeO_3$. Eqn (3.19) implies that in the Γ_4 phase the shear elastic, d (quasiferromagnetic), and two f branches are coupled. Expression (3.20) for the frequency ω_{III} of the shear elastic x-polarised vibration branch can be written near the transition as

$$\omega_{III}=\frac12\left\{\omega^2_{tk}-\frac{\omega^2_{ac}(1-\zeta_{df})^2}{\Lambda^2}+\left[\left(\omega^2_{tk}+\frac{\omega^2_{ac}(1-\zeta_{df})^2}{\Lambda^2}\right)^2-\frac{4\omega^2_{tk}\omega^2_{ac}\zeta_{de}(1-\zeta_{df})}{\Lambda^2}\right]^{1/2}\right\}^{1/2}, \tag{4.1}$$

where

$$\Lambda=\Lambda_d+\frac{\Lambda_f\omega_{2df}}{\omega_{5f}}\,,\qquad \omega_{5f}=\frac{qN(\lambda'_5+4\pi N\mu_5^2)}{M_B}\,,$$

$$\zeta_{de}=\frac{\omega_{me5}}{\omega_{ac}}\,,\qquad \zeta_{df}=\frac{\omega_{2df}}{\omega_{ac}}\,.$$

This expression simplifies considerably in the limiting cases of a high and low attenuation Λ in the d and f subsystems, to give

$$\omega_{III}=\omega_{tk}\begin{cases}\sqrt{1-\dfrac{\omega^2_{ac}\zeta_{de}(1-\zeta_{df})}{\Lambda^2\omega^2_{tk}}}\,, & \omega_{tk}\Lambda\gg\omega_{ac}(1-\zeta_{df}),\\ \sqrt{\dfrac{1-\zeta_{df}-\zeta_{de}}{1-\zeta_{df}}-\dfrac{\omega^2_{tk}\zeta^2_{de}\Lambda^2}{\omega^2_{ac}(1-\zeta_{df})^4}}\,, & \omega_{tk}\Lambda\ll\omega_{ac}(1-\zeta_{df}).\end{cases} \tag{4.1a}$$

The velocity $\tilde s_5=\omega_{III}/k$ of the mode at precisely the transition point $K_{ac}=0$ has the form

$$\tilde s_5=s_5\begin{cases}\sqrt{1-\dfrac{\omega_{me5}(Dk^2+\omega_{me5})}{\Lambda^2\omega^2_{tk}}}\,, & \omega_{tk}\Lambda\gg\omega_{me5}\,,\\ \sqrt{\dfrac{Dk^2}{Dk^2+\omega_{me5}}-\dfrac{\omega^2_{tk}\omega^2_{me5}\Lambda^2}{(Dk^2+\omega_{me5})^4}}\,, & \omega_{tk}\Lambda\ll\omega_{me5}\,,\end{cases} \tag{4.2}$$

where $D=g\alpha/M_0$. The attenuation coefficient $\gamma=\operatorname{Im}k(\omega)$ [7] of the quasielastic mode ω_{III} near the transition is given by

$$\gamma_{III}=\frac{\omega_{me5}\omega^2\Lambda^2}{s_5}\times\big[(\omega_{ac}-\omega_{2df}-\omega_{me5})(\omega_{ac}-\omega_{2df})+\omega^2\Lambda^2\big]^{-3/2}\times\big[(\omega_{ac}-\omega_{2df})^2+\omega^2\Lambda^2\big]^{-1/2}. \tag{4.3}$$

Eqns (4.1)–(4.3) imply that in the approximation we use $(\hat B^{(1)}=\hat B^{(2)}=0)$ the only way the f subsystem influences the quasielastic wave behaviour near the RPT point is through the terms responsible for the attenuation in the subsystem. Since the f subsystem at $T\gtrsim T_1$ is in a paramagnetic state, its attenuation is high (the line width being temperature dependent even at high temperatures of the order of the frequency itself [37, 69]) and may affect significantly the quasielastic branch behaviour at and around the $\Gamma_4-\Gamma_{24}$ RPT point.

The remaining branches are activation ones. We present here their activation and line width values in the linear approximation in the attenuation parameters Λ_d and Λ_f

($\Lambda_f \gg \Lambda_d$). In the case $\omega_{20} > \omega_{2f}$, the activation and line width of the quasiferrous branch ω_I at the RPT point are determined by interactions within the d subsystem, ME coupling (ME gap), the interaction between the d and f subsystems, and the dipole interaction, thus

$$\omega_I^2(0) = \omega_E(\omega_{me5} + \omega_{2df} + \omega_{dip}),$$
$$\Delta\omega_I = \Lambda_d\,\omega_E + \frac{\Lambda_f f_z^2 \omega_{2df}\,\omega_{5f}}{\omega_{me5} + \omega_{2df} + \omega_{dip}}. \quad (4.4)$$

In the case $\omega_{20} < \omega_{2f}$, the activation of this branch is determined by interactions within the d subsystem and by the ME and dipole interactions, and the line width, also by the d–f coupling

$$\omega_I^2(0) = \omega_E(\omega_{me5} + \omega_{dip}),$$
$$\Delta\omega_I = \Lambda_d(\omega_E + \omega_{me5} + \omega_{dip}) + \frac{\Lambda_f\,\omega_E\omega_{2df}}{\omega_{5f}}. \quad (4.5)$$

In the former case the activation and line width of the quasirare-earth mode ω_{II} at the RPT point are determined by the ME and dipole interactions as well as by the interactions within the f subsystem and between the d and f subsystems,

$$\omega_{II}^2(0) = \frac{\omega_{2f}^2}{\omega_{20}^2}\,\omega_E(\omega_{me5} + \omega_{dip}),$$
$$\Delta\omega_{II} = \Lambda_f f_z^2\left(\omega_{4f} + \omega_{5f} - \frac{\omega_{5f}\,\omega_{2df}}{\omega_{me5} + \omega_{2df} + \omega_{dip}}\right), \quad (4.6)$$

and in the latter case, by interactions within the f subsystem, by the coupling of the d and f subsystems, and by the dipole interaction [terms $\sim 4\pi N\mu_i^2$ in the coefficients $\tilde{\lambda}_i$ in (A.2)], so that

$$\omega_{II}^2(0) = \omega_{2f}^2 + \omega_E\omega_{2df},$$
$$\Delta\omega_{II} = \Lambda_f\left[f_z^2(\omega_{4f} + \omega_{5f}) - \frac{\omega_E\omega_{2df}}{\omega_{5f}}\right], \quad (4.7)$$

where $\omega_{4f} = gN\lambda_4/M_B$. The spectrum of coupled vibrations at this RPT is shown schematically in Fig. 16.

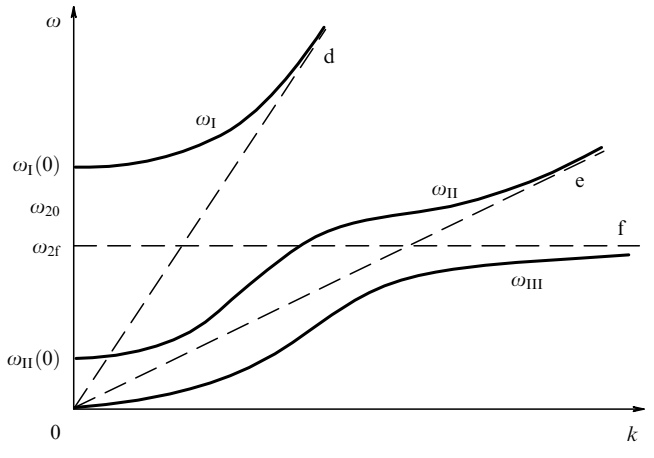

Figure 16. Schematic diagram of the spectrum of coupled ME vibrations at the $\Gamma_4 - \Gamma_{24}$ RPT point (in the absence of attenuation) for $\omega_{20} > \omega_{2f}$. Dashed lines show the uncoupled vibration branches of the d, f, and elastic subsystems. For the $\omega_{20} < \omega_{2f}$ case one should make the replacement $\omega_I \rightleftarrows \omega_{II}$ and place ω_{20} on the axis of ordinates between ω_{2f} and ω_I.

We now proceed to numerical estimates taking from the data of Refs [12, 19–22, 30, 36, 52, 71] the values of the parameters of interest. For erbium orthoferrite these values are

$$M_0 \approx 830\ \text{Oe}, \quad \rho \approx 8\ \text{g cm}^{-3}, \quad A \approx 8.8 \times 10^9\ \text{erg cm}^{-3},$$
$$B_x \approx 0.6\ \text{K}, \quad B_y = 1.3\ \text{K}, \quad B_z'' = 2.4\ \text{K},$$
$$|\lambda_i| \approx 3\ \text{K}, \quad c_{55} \approx 8.9 \times 10^{11}\ \text{erg cm}^{-3},$$
$$c_{44} \approx 1.2 \times 10^{12}\ \text{erg cm}^{-3}, \quad d \approx 8.8 \times 10^7\ \text{erg cm}^{-3},$$
$$B_{55} \approx 2 \times 10^6\ \text{erg cm}^{-3}, \quad (4.8)$$

and for ytterbium orthoferrite

$$M_0 \approx 807\ \text{Oe}, \quad \rho \approx 8\ \text{g cm}^{-3}, \quad A \approx 1.15 \times 10^{10}\ \text{erg cm}^{-3},$$
$$B_x \approx 3.35\ \text{K}, \quad B_z'' = 5.2\ \text{K}, \quad |\lambda_i| \approx 3\ \text{K},$$
$$c_{55} \approx 8.7 \times 10^{11}\ \text{erg cm}^{-3}, \quad c_{44} \approx 1.1 \times 10^{12}\ \text{erg cm}^{-3}. \quad (4.9)$$

Note that the ME constant B_{55} of erbium orthoferrite was found [20] by comparing the theoretical and experimental behaviours of the transversal sound velocity s_5 near the $\Gamma_4 - \Gamma_{24}$ and $\Gamma_2 - \Gamma_{24}$ RPTs. However, the theoretical formulas used in Ref. [20] for sound wave velocity in the RPT region cannot be considered entirely adequate in describing experimental results, due in particular to the neglect of spontaneous and dynamic deformations in the material [7]. This is especially true of the RPT points themselves. We will therefore improve this estimate based on the later theoretical [26] and experimental [19, 30] results, the former being represented by Eqns (4.1)–(4.3) and the latter shown in Figs 1 and 5. A calculation using experimental data on the sound velocity change $\Delta s/s$ [19] and Eqns (3.20) or (4.1a) for $\Lambda = 0$, $K_{ac} = (6T - 600) \times 10^3$ erg cm^{-3}, and $K_{ac} + K_2 = (6T - 540) \times 10^3$ erg cm^{-3} [20, 30] yields $B_{55} \approx 6.5 \times 10^6$ erg cm^{-3} for erbium orthoferrite. In a similar way, the experimental data on $\Delta s/s$ [12] may be used to obtain the ME constant B_{55} for ytterbium orthoferrite. Using the data of Ref. [30] and theoretical results (3.10) and (3.11), which imply

$$K_{ac} = \left[4.13 - 7.2\tanh\left(\frac{5.2}{T}\right)\right] \times 10^6\ \text{erg cm}^{-3},$$
$$K_{ac} + K_2 = \left[4.66 - 7.2\tanh\left(\frac{5.2}{T}\right)\right] \times 10^6\ \text{erg cm}^{-3},$$

and setting $\Lambda = 0$ in (3.20) or (4.1a) one obtains $B_{55} \approx 2 \times 10^7$ erg cm^{-3} for $YbFeO_3$.

To compare experimental and theoretical results on the coupled wave behaviour near an RPT requires a knowledge of the exact attenuation parameters in the d and f subsystems (Λ_d and Λ_f) in each particular REOF. Because of the lack of these, we will proceed as follows to make quantitative estimates. For the attenuation parameter in the d subsystem we order $\Lambda_d = 10^{-4}$ [30, 69] based on the experimental fact that the line width to frequency ratio in the d subsystem is $\sim 10^{-2}$ [69]. The attenuation parameter in the f subsystem can also be estimated from the experimental fact that, when in the paramagnetic state, the mode line width in the f subsystem depends on the temperature and is of the order of the frequency itself [30, 69]. Thus, we conclude finally that in $ErFeO_3$ $\Lambda_f \sim 50 - 100$ and in $YbFeO_3$ $\Lambda_f \sim 1 - 5$.

Using the problem parameter values (4.8) and (4.9) we can estimate the frequencies entering (4.1)–(4.7) at the RPT point $\Gamma_4-\Gamma_{24}$ ($T=T_1,\ K_{ac}(T_1)=0$).

In $ErFeO_3$

$$\begin{aligned}
&\omega_E \approx 2.25\times10^{14}\ s^{-1}, \quad && \omega_{2f} \approx 1.5\times10^{11}\ s^{-1},\\
&\omega_{20} \approx 8.6\times10^{11}\ s^{-1}, && \omega_{2df} \approx 3\times10^{9}\ s^{-1},\\
&\omega_{dip} \approx 7.3\times10^{7}\ s^{-1}, && \omega_{5f} \approx 2.5\times10^{13}\ s^{-1},\\
&\omega_{me5} \approx 10^{6}\ s^{-1}. &&
\end{aligned} \tag{4.10}$$

In $YbFeO_3$

$$\begin{aligned}
&\omega_E \approx 2.5\times10^{14}\ s^{-1}, \quad && \omega_{2f} \approx 8.8\times10^{11}\ s^{-1},\\
&\omega_{20} \approx 5.5\times10^{12}\ s^{-1}, && \omega_{2df} \approx 1.2\times10^{11}\ s^{-1},\\
&\omega_{dip} \approx 7.3\times10^{7}\ s^{-1}, && \omega_{5f} \approx 2.6\times10^{12}\ s^{-1},\\
&\omega_{me5} \approx 10^{7}\ s^{-1}. &&
\end{aligned} \tag{4.11}$$

Here it is assumed that ytterbium and erbium orthoferrites have constants d of equal magnitude.

Given the frequency estimates (4.10) and (4.11) and the attenuation parameters Λ_d and Λ_f, one can compare the experimental and theoretical results of Sections 1 and 2 on the coupled wave behaviour at the $\Gamma_4-\Gamma_{24}$ RPT point.

Let us first consider the behaviour of the sound velocity $\tilde{s}_5$ (4.2) at the transition point. From (4.10) and (4.11) it follows that even at the frequency $\nu=25$ MHz (the lowest used in the experiment) the leading term in the brackets in (4.2) is the attenuation term proportional to $\omega^2\Lambda^2$. Using the parameter values listed above, it is found that in erbium orthoferrite the fractional velocity change $\Delta s_5/s_5=(s_5-\tilde{s}_5)/s_5$ at this frequency is about 10% and that in ytterbium orthoferrite, at $\nu=54$ GHz, this quantity is 1%. These values are somewhat large relative to the experimental ones (see Figs 1 and 5), indicating that our estimates of the constants λ_i, Λ_d, Λ_f are rather crude.

Note that the increase in $\Delta s_5/s_5$ at $T=T_1$ in $YbFeO_3$ in a magnetic field $\mathbf{H}\parallel\mathbf{z}$ (see Fig. 6) can be accounted for by the decrease in the attenuation coefficient Λ_f upon magnetic-field-induced ordering of the f subsystem at a sufficiently low temperature $T_1\approx 8$ K. In $ErFeO_3$ $T_1\sim 100$ K, and the ordering effect of the magnetic field on the f subsystem is small. Presumably this is the reason why a magnetic field suppresses the large change in $\Delta s_5/s_5$ (see Fig. 2).

For both of these orthoferrites, it follows from (4.10) and (4.11) that in the $\Gamma_4-\Gamma_{24}$ RPT region we have the condition $\omega_{20}>\omega_{2f}$ and that the soft mode is the f one ω_{II}. The activation of this mode at the RPT point is determined by (4.6). Given the above ME constants, we have $\nu_{II}(0)\approx 4$ GHz in erbium orthoferrite, and $\nu_{II}(0)\approx 5$ GHz in ytterbium orthoferrite. The latter value agrees to the order of magnitude with the experimental $\nu_{II}(0)\approx 20$ GHz (see Figs 3, 4) (the difference may be due to the lack of an exact estimate for the constant d in ytterbium orthoferrite). The soft mode gap in erbium orthoferrite evaded experimental measurement [14, 15, 61] because of there being a single absorption signal at the RPT point in this material (see Fig. 1). The possible reason is, as already discussed, the large attenuation in the f subsystem at high temperatures ($T_1\approx 100$ K in erbium orthoferrite). In ytterbium orthoferrite $T_1\approx 10$ K, therefore attenuation in the f subsystem is much lower and two absorption lines are detected, enabling the soft mode gap to be measured.

4.1.2 $\Gamma_2-\Gamma_{24}$ transition in $ErFeO_3$ and $YbFeO_3$. Near this RPT, it follows from (3.22b) that the coupled branches are the quasiferromagnetic branch of the d subsystem, one of the branches of the f subsystem, and the transversal x-polarised sound. At the RPT point $T=T_2$ ($K_{ac}+K_2=0$) the quasielastic branch ω_{III} (3.20) behaves differently than at the $\Gamma_4-\Gamma_{24}$ transition due to the dipole interaction effect [7]. Thus, the velocity of this vibration branch at exactly the transition point ($T=T_2$) is given by

$$\tilde{s}_5 = s_5\begin{cases}\sqrt{1-\dfrac{\omega_{me5}(Dk^2+\omega_{me5}+\omega_{dip})}{\Lambda^2\omega_{tk}^2}}, & \omega_{tk}\Lambda\gg\omega_{me5}+\omega_{dip},\\ \sqrt{\dfrac{Dk^2+\omega_{dip}}{Dk^2+\omega_{me5}+\omega_{dip}}-\dfrac{\omega_{tk}^2\omega_{me5}^2\Lambda^2}{(Dk^2+\omega_{me5}+\omega_{dip})^4}}, & \omega_{tk}\Lambda\ll\omega_{me5}+\omega_{dip}.\end{cases} \tag{4.12}$$

The activations of the remaining two branches of coupled vibrations at the $\Gamma_2-\Gamma_{24}$ RPT point are given by the first equations in (4.4)–(4.7).

Now let us return to the comparison of theory and experiment. Again using the erbium and ytterbium orthoferrite constants (4.7) and (4.8), the frequencies entering (4.4)–(4.7) and (4.12) are estimated as follows. In erbium orthoferrite

$$\begin{aligned}
&\omega_{2f} \approx 6\times10^{11}\ s^{-1}, \quad && \omega_{20} \approx 3.4\times10^{11}\ s^{-1},\\
&\omega_{2df} \approx 2.2\times10^{8}\ s^{-1}, && \omega_{5f} \approx 2.3\times10^{13}\ s^{-1}.
\end{aligned} \tag{4.13}$$

In ytterbium orthoferrite

$$\begin{aligned}
&\omega_{2f} \approx 1.4\times10^{12}\ s^{-1}, \quad && \omega_{20} \approx 3.9\times10^{12}\ s^{-1},\\
&\omega_{2df} \approx 6\times10^{10}\ s^{-1}. &&
\end{aligned} \tag{4.14}$$

The remaining frequencies are given by (4.10) and (4.11), respectively. The attenuation parameters in the d and f subsystems near the $\Gamma_2-\Gamma_{24}$ RPT may be set equal to those near the $\Gamma_4-\Gamma_{24}$ transition [69]. Then, for both erbium and ytterbium orthoferrites, the leading term in (4.12) at frequency $\nu\lesssim 50$ MHz is ω_{dip}. From (4.13) and (4.14), the fractional sound velocity change at these frequencies is about 1–5% in either REOF. While for erbium orthoferrite this is consistent with experiment (see Fig. 1), ytterbium orthoferrite exhibits a discrepancy (see Fig. 5), which can probably again be explained by the crude estimates for the constants λ_i and Λ_f.

From (4.13) and (4.14) it follows that in $ErFeO_3$ $\omega_{2f}>\omega_{20}$, and the soft mode near $\Gamma_2-\Gamma_{24}$ RPT is the d subsystem quasiferromagnetic mode ω_I. In $YbFeO_3$ $\omega_{20}>\omega_{2f}$, and the soft mode is, as before, the f subsystem mode ω_{II}. The activation of these modes at the RPT point $T=T_2$ is determined, for $ErFeO_3$, by the first equation in (4.5) [$\nu_I(0)\approx 21$ GHz], and for $YbFeO_3$, by the first equation in (4.6) [$\nu_{II}(0)\approx 8$ GHz]. Both values, especially that for erbium orthoferrite, agree in order of magnitude with experimental ones (see Figs 1, 4). The fact that it is a d subsystem mode which is soft in $ErFeO_3$ at $T=T_2$ (rather than a f subsystem mode as at $T=T_1$) is confirmed by its being well resolved in experiment. For the f mode at $T=T_2\approx 90$ K, attenuation is again large, and it should not therefore be resolvable (as for $T=T_1$).

4.1.3 $\Gamma_2-\Gamma_{12}$ transition in $ErFeO_3$. From Eqn (3.22a) it follows that near this transition the quasiferromagnetic

branch of the d subsystem, one f mode, and the shear y-polarised elastic branch are coupled. The quasielastic branch $\omega_{\rm III}$ (3.20) and its attenuation coefficient near the RPT point $K_{cb}(T_{\rm N2}) = 0$ are obtained from Eqns (4.1) and (4.3) by making the index replacements $2 \to 1$, $5 \to 4$, $ac \to cb$. The velocity of this branch $\tilde{s}_4 = \omega_{\rm III}/k$ at exactly the transition point is given by (4.2) with the same index replacements. Note that, unlike the $\Gamma_2 - \Gamma_{24}$ transition at $T = T_{\rm N2}$, the dipole interaction does not affect the behaviour of the quasielastic mode $\omega_{\rm III}$ [see (3.20) and (A.3)]. Since the $\Gamma_2 - \Gamma_{12}$ transition is observed at low temperatures, the f subsystem attenuation is expected to be lower than near $\Gamma_4 - \Gamma_{24}$ and $\Gamma_2 - \Gamma_{24}$ transitions (by at least an order of magnitude [69], so that $\Lambda_{\rm f} \lesssim 1$ at $T \sim T_{\rm N2}$). Due to these two factors (i.e., no effect of the dipole interaction at $T = T_{\rm N2}$, and the reduced f subsystem attenuation at low temperatures), the change in the transversal sound velocity $\tilde{s}_4$ near the $\Gamma_2 - \Gamma_{12}$ RPT will exceed that at $\Gamma_2 - \Gamma_{24}$ and $\Gamma_4 - \Gamma_{24}$ transitions. Experimentally [14–19, 61], a sound velocity change at $T = T_{\rm N2}$ of more than 20% has been reported (see Fig. 9), the first time ever that large in a REOF.

Near the $\Gamma_2 - \Gamma_{12}$ transition (assuming, as shown below, that the low-temperature ME constant B_{44} is by at least an order of magnitude larger that its high-temperature value), Eqn (4.8) yields the following estimates for the frequencies involved in (3.22a) for erbium orthoferrite:

$$\omega_{\rm 1f} \approx 6.3 \times 10^{11}\ {\rm s}^{-1}\,, \qquad \omega_{10} \approx 1.8 \times 10^{12}\ {\rm s}^{-1}\,,$$
$$\omega_{\rm 1df} \approx 1.5 \times 10^{10}\ {\rm s}^{-1}\,, \qquad \omega_{\rm 4f} \approx 1.6 \times 10^{12}\ {\rm s}^{-1}\,,$$
$$\omega_{\rm me4} \approx 10^{9}\ {\rm s}^{-1}\,. \tag{4.15}$$

With these estimates, it is found from (4.2) that at the $\Gamma_2 - \Gamma_{12}$ point in erbium orthoferrite the relative change in the transversal sound velocity $\tilde{s}_4$ must exceed 90%. The experimentally observed change was more than 20% up to the disappearance of the echo pattern (see Fig. 9). The absence of echo signals at approaching the RPT point is explained by the fact that, according to (4.3), the sound attenuation coefficient near the RPT increases strongly due to the resonance factor in the first bracket.

From (4.15) it is seen that at $T = T_{\rm N2}$ $\omega_{10} > \omega_{\rm 1f}$, and the soft mode near this transition is the quasirare-earth mode, whose activation is given by an expression similar to the first equation in (4.6) for $\omega_{\rm dip} = 0$, thus

$$\omega_{\rm II}^2(0) = \left(\frac{\omega_{\rm 1f}}{\omega_{10}}\right)^2 \omega_{\rm E}\omega_{\rm me4}\,. \tag{4.16}$$

From this, the estimate for the soft mode gap at $T = T_{\rm N2}$ is $\nu_{\rm II}(0) \sim 25$ GHz, which is consistent with experiment [8, 15] (see Fig. 9).

One further feature observed near the $\Gamma_2 - \Gamma_{12}$ transition is that the soft mode behaviour and acoustic parameters are sharply asymmetric about the transition point (see Fig. 9). The reason is that both the effective f–f interaction constants and the anisotropy constants depend on the temperature differently to the right and to the left of $T_{\rm N2}$. Let us demonstrate that the temperature dependence of these constants is indeed different in various temperature intervals. Near high-temperature transitions, when the f subsystem is paramagnetic (meaning that $f, c, \sigma \ll 1$), we have $\operatorname{artanh}\sigma \approx \sigma$ and hence, according to (3.8a), $\lambda_i' \approx T - \lambda_i \approx T$ (since at high temperatures $T \gg \lambda_i$ [37, 69]). From (3.10) and (3.12),

$$K_{ac} = \tilde{K}_{ac}(T) - \frac{N(B_z'^2 + B_z''^2 - B_x^2)}{T}\,,$$
$$K_{cb} = \tilde{K}_{cb}(T) + \frac{N(B_z'^2 + B_z''^2 - B_y^2)}{T}\,, \tag{4.17}$$

where the temperature dependence of the anisotropy constants $K_{ac,\,cb}$ is determined by the temperature dependence of their van Fleck [30, 37, 69] and ME components.

As a consequence, given the experimental data [20, 30] on erbium orthoferrite in the spin reorientation $\Gamma_4 - \Gamma_{24} - \Gamma_2$ temperature range, the anisotropy constant K_{ac} depends linearly on T:

$$K_{ac} = \left|0.238 - 2.44 \times 10^{-3} T\right|\ {\rm K}\,. \tag{4.18}$$

Near the $\Gamma_2 - \Gamma_{12}$ RPT (at $T \gtrsim T_{\rm N2}$) the f subsystem is nearly ordered, so that $f, c, \sigma \sim 1$. In order to find the temperature dependence of the constants λ_i' and K_{cb} for $T \gtrsim T_{\rm N2}$, assume for the sake of simplicity that $a = B_z'' = \lambda_{7,8} = 0$ and $B_z' \gg \lambda_i\sigma$. It then follows from (3.8) that in the Γ_2 phase

$$f_z = c_y = 0\,, \qquad f_x = \sigma = \frac{B_z'}{\lambda_1'}\,,$$

and from (3.8a) that

$$\operatorname{artanh}\sigma \approx \frac{B_z'}{T}\,, \qquad \text{i.e.,} \qquad f_x = \tanh\left(\frac{B_z'}{T}\right).$$

Substituting these results into (3.8a) for λ_i', and (3.10) and (3.12) for $K_{ac,\,cb}$, it is found that, for $T \gtrsim T_{\rm N2}$,

$$\lambda_i' \approx B_z' \tanh^{-1}\left(\frac{B_z'}{T}\right),$$
$$K_{ac,\,cb} \approx \tilde{K}_{ac,\,cb}(T) \mp \frac{N(B_z'^2 - B_{x,y}^2)}{B_z'} \tanh\left(\frac{B_z'}{T}\right). \tag{4.19}$$

Here the constants $\tilde{K}_{ac,\,cb}$ may depend on the temperature only through the ME contribution, since the van Fleck contribution is virtually constant at low temperatures [30]. Using the experimental data [14–19, 30, 36] we finally obtain from (4.7) the following expression for K_{cb} in erbium orthoferrite for $T \gtrsim T_{\rm N2}$:

$$K_{cb} = \left[3.37 - 6.42 \tanh\left(\frac{2.4}{T}\right)\right]\ {\rm K}\,. \tag{4.20}$$

At $T \lesssim T_{\rm N2}$ the f subsystem is ordered. In this case the temperature dependence of the f–f and f–d interaction parameters must change again, which will also result in a different temperature dependence of the anisotropy constants in the temperature range $T \lesssim T_{\rm N2}$.

Thus, the soft mode asymmetry in the $\Gamma_2 - \Gamma_{12}$ RPT region may indeed be explained by the fact that both the effective f–f and f–d interaction constants and the anisotropy constants have different temperature dependence to the right and to the left of $T_{\rm N2}$.

Knowledge of the temperature dependence of anisotropy constants makes it possible to determine the ME constants B_{55} and B_{44} at various temperatures based on the experimental dependence of the quasisound velocities (3.20),

$\tilde{s}(T) = \omega_{III}(T)/k$ [14–20, 61]. For erbium orthoferrite near high temperature transitions, the values $B_{55} \approx 2.2 \times 10^6$ erg cm^{-3} and $B_{44} \approx 4 \times 10^6$ erg cm^{-3} have been obtained [20]. Using the experimental dependence of the velocity of the transversal y-polarised sound [14–19, 61] and the above T dependence of the anisotropy constant K_{cb} near the $\Gamma_2-\Gamma_{12}$ RPT at $T \gtrsim T_{N2}$, we obtain from (3.20) or (4.1a) for $\Lambda = 0$ that the ME constant B_{44} at low temperatures increases by nearly two orders: $B_{44} \approx 2.5 \times 10^8$ erg cm^{-3}. Presumably, such a significant increase in the ME constant B_{44} near the $\Gamma_2-\Gamma_{12}$ RPT may be accounted for by the fact that at low temperatures the contribution to the ME energy from the f subsystem increases because of this latter being almost ordered. Thus, if one takes into account the f–d-interaction-related magnetostriction (3.6b), all the relevant formulas must be used with the ME constant B_{44} replaced by $\tilde{B}_{44}$ defined by

$$\tilde{B}_{44} = B_{44} + B^{(1)}_{1223} f_x + B^{(2)}_{2233} c_y + \frac{B^{(2)}_{3323} B_y}{\lambda'_6} . \qquad (4.21)$$

Thus, if at high temperatures the value of $\tilde{B}_{44}$ is mainly determined by the first term in (4.21), at low temperatures the last three terms appear to dominate.

The fact that the constants B_{55} and B_{44} and the temperature behaviour of the anisotropy constants depend on the type of the transition ($\Gamma_4-\Gamma_{24}$, $\Gamma_2-\Gamma_{24}$, or $\Gamma_2-\Gamma_{12}$) may also explain the difference in the amount of change in the sound velocity at these transitions at low attenuation in the f subsystem. Indeed, assuming (4.18) to hold near the $\Gamma_4-\Gamma_{24}$ and $\Gamma_2-\Gamma_{24}$ transitions, a twofold sound velocity reduction is expected within

$$\Delta T \approx \frac{M_0 \omega_{me5}}{g\, \partial K_{ac}/\partial T} \sim 10^{-4}-10^{-3} \text{ K}$$

of the RPT. Thus, one must come very close the RPT point to be able to observe large sound velocity changes near high-temperature transitions. Near the $\Gamma_2-\Gamma_{12}$ transition, the same amount of reduction will be observed at

$$\Delta T \approx \frac{M_0 \omega_{me4}}{g\, \partial K_{cb}/\partial T} \sim 10^{-2}-10^{-1} \text{ K},$$

a quite achievable proximity experimentally.

The above-mentioned ($\Gamma_2-\Gamma_{12}$) RPT in erbium orthoferrite is unique among temperature transitions for displaying such a strong change in the sound velocity.

Thus, based on the above theoretical study of the coupled vibrations of the rare-earth, iron, elastic, and dipole subsystems in Kramers ion REOFs; and comparing the predictions with experiment, the following conclusions can be made.

Depending on the relationship between the f subsystem vibration frequency and the d subsystem vibration frequency renormalised by the interaction with the f, elastic, and dipole subsystems, either one of the quasiferrous modes or one of the quasirare-earth modes may be soft in the region near a reorientation phase transition. Thus, for example, in erbium orthoferrite near the $\Gamma_4-\Gamma_{24}$ and $\Gamma_2-\Gamma_{12}$ transitions the soft mode is the quasirare-earth one, and near the $\Gamma_2-\Gamma_{24}$ transition, the quasiferromagnetic one. In ytterbium orthoferrite, the f subsystem mode is soft near both transitions ($\Gamma_4-\Gamma_{24}$ and $\Gamma_2-\Gamma_{24}$).

In the region of the $\Gamma_4-\Gamma_{24}$ RPT, the small change in the velocity of the transversal x-polarised sound may be due to the large attenuation coefficient in the paramagnetic f subsystem (the line width is temperature dependent even at high temperatures of the order of the frequency itself [37, 69]), which coefficient enters the sound attenuation expression (4.3). The attenuation coefficient may be so large as to suppress echo signals near the transition point [24]. Another factor to explain the small sound velocity change is that the significant (twofold and more) velocity reduction near T_1 occurs in an extremely narrow ($10^{-4}-10^{-3}$ K) and experimentally unresolvable temperature interval.

Near the $\Gamma_2-\Gamma_{24}$ phase transition, the small sound velocity change is due primarily to the effect of the dipole interaction which results from the wave vector being noncollinear with the ferromagnetism vector (4.12).

Near the low-temperature phase transition $\Gamma_2-\Gamma_{12}$ in erbium orthoferrite, the experimentally reported $> 25\%$ reduction in the velocity of y-polarised sound may be explained, first, by the significant reduction on the f subsystem attenuation at low temperatures, and second, by the fact that near this transition the magnitude of the sound velocity change is not restricted by the dipole interaction. One further observed feature, the weak temperature dependence of the soft mode frequency near the $\Gamma_2-\Gamma_{12}$ transition, is explained by the fact that the temperature dependence of the anisotropy constants, Eqns (4.17) and (4.19), may undergo a significant change at low temperatures. This, in turn, has a consequence that the temperature 'proximity' interval at the RPT point increases to tenths of a degree, which makes this transition unique because no proximity interval of this size has yet been found in any magnetic material.

The estimated values of the soft mode gaps in the RPT region agree to the order of magnitude with the experimental data. To confirm our conclusions and perform a more accurate comparison of theory and experiment, further experiments are needed to determine the temperature behaviour of the anisotropy constants and the values of the ME, f–f, and d–f coupling constants.

4.2 Coupled vibrations in rare-earth orthoferrites with non-Kramers rare-earth ions near phase transitions

Although the non-Kramers ions Tm^{3+} and Ho^{3+} stand next to one another as to the number of 4f electrons (12 and 10, respectively), they differ greatly in dynamic properties. This is seen, in particular, by comparing the dependences presented in Figs 12–15. We shall here discuss the known experimental data in terms of the dynamic interaction of the magnetic and elastic subsystems.

The simplest and qualitatively predictable situation occurs in $TmFeO_3$. In it, a high-frequency absorption has been found on either reorientation boundary, which is definitely linked to the softening magnetoresonance mode having energy gaps at T_1 and T_2. At the same points, a reduction (if insignificant) in the velocity of the active sound wave occurs. Thus, the behaviour of the soft magnetic and acoustic modes is in qualitative agreement with the notion of magnetoelastic coupling. A more complex situation obtains in $HoFeO_3$, where the $\Gamma_2-\Gamma_4$ RPT structure is not quite simple either. Here the gaps at reorientation boundaries are not measurable and can only be estimated by calculation. As for sound experiments, these yield also quantitative results, even though the relevant effects at the $\Gamma_{24}-\Gamma_4$ transition in $HoFeO_3$ are even smaller than in $TmFeO_3$. Thus, the active sound velocity changes at T_1 have very low values of order 10^{-4} for the mode with $\mathbf{k} \parallel \mathbf{a}$, $\mathbf{u} \parallel \mathbf{c}$, and of 7×10^{-4} for the

wave with $\mathbf{k} \parallel \mathbf{c}$, $\mathbf{u} \parallel \mathbf{a}$. At the same time, the resonant change in the mode with $\mathbf{k} \parallel \mathbf{c}$, $\mathbf{u} \parallel \mathbf{b}$ velocity at the lower-temperature ($T = T_3$) reorientation boundary is relatively large ($\sim 3 \times 10^{-2}$). Thus, experiment shows that the magnetoelastic coupling strengths at T_1 and T_3 differ by two orders of magnitude.

We shall now analyse the existing experimental data using the theory developed above. We note, as a preliminary, that the theory of Section 3.2 is only valid for REOFs with quasidoublet non-Kramers ions such as terbium or holmium ions, for example. The structure of the thulium ion is more complicated [30, 36]. In this case, the analysis of the vibration spectrum will rely on the same theoretical results with the only difference that the effect of the f subsystem is reduced to the renormalisation of d subsystem parameters (without specifying the way in which they are affected by the f ions). This approach is valid since in thulium orthoferrite the frequencies of the f mode exceed those of the d mode, $\omega_{1f,2f} > \omega_{10,20}$ [30].

4.2.1 $\Gamma_4 - \Gamma_{24}$ transition in $TmFeO_3$ and $HoFeO_3$. Near this RPT, (3.30) implies that, since $G_z \approx 0$, the branches ω_{III}, ω_{IV}, and ω_V are virtually identical to the uncoupled branches ω_{1k}, ω_{4k}, and ω_{3k}. The branch ω_{VI}, corresponding to the shear quasielastic (x-polarised) vibration branch, does differ from the uncoupled branch ω_{5k}. Near the transition point ($T = T_1$, $G_z = 0$, $K_{ac} = 0$), in the long wavelength approximation the mode ω_{VI} and its attenuation γ_{VI} are expressed by (4.1) and (4.3) with indices III replaced by VI, and 5f by f′. The velocity $\tilde{s}_5 = \omega_{VI}/k$ of this mode at the RPT point is given by (4.2). The remaining two branches are activation ones, their activations for $\omega_{20} > \omega_{2f}$ and $\omega_{20} < \omega_{2f}$ being determined by Eqns (4.4)–(4.7). At the $\Gamma_4 - \Gamma_{24}$ RPT point, it follows from these equations that at $\omega_{20} > \omega_{2f}$ the soft mode is the f mode, and at $\omega_{20} < \omega_{2f}$, the d mode. In the former case the soft mode activation may be either larger or smaller than the ME gap $\sqrt{\omega_E \omega_{me5}}$ [cf. (4.6)], whereas in the latter case it is always larger [cf. (4.5)]. In both cases the activation of the quasiferrous branch is larger than the ME gap. Therefore the gap seen in the spectra of the f or d modes cannot be identified with the ME gap.

We will now present some quantitative results taking from [24, 30, 37, 69] the magnitudes of the constants entering Eqns (4.1)–(4.7). In holmium orthoferrite

$$M_0 \approx 830 \text{ Oe}, \quad \rho \approx 8 \text{ g cm}^{-3}, \quad A = 1.3 \times 10^{10} \text{ erg cm}^{-3},$$
$$\Delta_{ex}^0 = 4.7 \text{ K}, \quad \Delta_{CF} = 2.4 \text{ K}, \quad \lambda_f = -3.5 \text{ K},$$
$$\lambda_c = -2.5 \text{ K}, \quad \mu_x = 3.25\mu_B, \quad \mu_y = 7.2\mu_B,$$
$$d = 10^8 \text{ erg cm}^{-3}. \tag{4.22}$$

In thulium orthoferrite

$$M_0 \approx 816 \text{ Oe}, \quad \rho = 8.16 \text{ g cm}^{-3}, \quad A = 1 \times 10^{10} \text{ erg cm}^{-3},$$
$$d \approx 1.5 \times 10^8 \text{ erg cm}^{-3}, \quad c_{55} \approx 9.2 \times 10^{11} \text{ erg cm}^{-3},$$
$$c_{44} \approx 1.1 \times 10^{12} \text{ erg cm}^{-3}. \tag{4.23}$$

Of the ME constants, only the constant B_{55} in thulium orthoferrite is available [24], $B_{55} = 4.4 \times 10^7$ erg cm^{-3}. As already mentioned, earlier studies (including [24]) have not employed entirely exact formulas in deriving ME constants from the sound velocity behaviour near the RPT. Using the more recent results (4.5) and (4.1) and the experimental data of Ref. [24] (see Fig. 13), and taking $K_{ac} + K_2 = (218.4 - 2.6T) \times 10^5$ erg cm^{-3}, the improved magnitude of the constant B_{55} for thulium orthoferrite is $B_{55} \approx 8 \times 10^7$ erg cm^{-3}. Since the experimental dependence of the sound velocity $\tilde{s}_5$ in $HoFeO_3$ in the $\Gamma_4 - \Gamma_{24}$ RPT region is unknown, we take $B_{55} \approx 10^7$ erg cm^{-3} in this material. The attenuation parameters will be taken to be $\Lambda_d \sim 10^{-4}$ and $\Lambda_f \sim 1 - 10$ [69].

For $HoFeO_3$, the frequencies involved in (4.1)–(4.7) are estimated to be

$$\omega_E \approx 2.8 \times 10^{14} \text{ s}^{-1}, \quad \omega_{2f} \approx \omega_f \approx \omega_{f'} \approx 6.5 \times 10^{11} \text{ s}^{-1},$$
$$\omega_{20} \approx 2.3 \times 10^{12} \text{ s}^{-1}, \quad \omega_{2df} \approx 2 \times 10^{10} \text{ s}^{-1},$$
$$\omega_{dip} \approx 4 \times 10^7 \text{ s}^{-1}, \quad \omega_{me5} \approx 4.6 \times 10^7 \text{ s}^{-1}, \tag{4.24}$$

and for $TmFeO_3$ (in which the magnetic constants are unknown and hence the frequencies ω_{2f}, ω_{20}, and ω_{2df} are not estimated),

$$\omega_E \approx 2.25 \times 10^{14} \text{ s}^{-1}, \quad \omega_{dip} \approx 1.51 \times 10^8 \text{ s}^{-1},$$
$$\omega_{me5} \approx 1.5 \times 10^8 \text{ s}^{-1}. \tag{4.25}$$

From a comparison of the experimental and theoretical results on the coupled wave behaviour near the $\Gamma_4 - \Gamma_{24}$ transitions the following picture emerges.

Estimates show that at frequencies near 50 MHz the terms ω_{me5} and $\omega\Lambda$ in (4.2) are of the same order, so that the fractional sound velocity change at the $\Gamma_4 - \Gamma_{24}$ RPT point is expected to be $\Delta s_5/s_5 \approx 10\%$. Experimentally, for thulium orthoferrite, a $\approx 3\%$ velocity reduction is observed (see Fig. 13) [24]. The exact magnitude of this reduction was not found, however, because of the large attenuation in the material (there were no echos near and above the RPT point). In holmium orthoferrite the experimental value of the fractional sound velocity change is $\sim 0.1\%$ [13]. A possible reason is that the ME constant B_{55} (frequency ω_{me5}) in this REOF is small compared to the similar constants in thulium orthoferrite (rather than of the same order as assumed above).

It follows from (4.24) that in holmium orthoferrite the condition $\omega_{20} > \omega_{2f}$ holds near the $\Gamma_4 - \Gamma_{24}$ transition, and so the soft mode is the quasirare-earth one. From (4.6), the activation of this mode at the RPT point is $\nu_{II}(0) \approx 5$ GHz. Note that the exact value of the soft mode activation in $HoFeO_3$ in the $\Gamma_4 - \Gamma_{24}$ RPT region has not been determined experimentally. Thus, frequencies $\omega/2\pi > 70$ GHz used in Refs [37, 69] imposed experimental limitations on the determination of the activation (which can in principle be lower than that). In Ref. [13], the soft mode activation could not be measured because only one absorption signal was present, a possible reason being that two absorption signals merged into one due to the large attenuation (of the order of the frequency itself [69]) in the paramagnetic f subsystem (see Fig. 14). The large attenuation in the f subsystem may also be a cause of one further effect, in the elastic subsystem this time. Analysis of Eqn (4.3) shows that for the transversal x-polarised sound γ_{VI}, which is coupled most strongly to the d subsystem, the attenuation coefficient is determined by both the d subsystem spin wave attenuation Λ_d and the f subsystem spin wave attenuation Λ_f. Since the f subsystem near this RPT is usually paramagnetic, the attenuation coefficient Λ_f is much larger than Λ_d ($\Lambda_d \sim 10^{-4}$, $\Lambda_f \sim 1 - 10$, and $\Lambda_d/\Lambda_f \sim 10^{-4} - 10^{-5}$ [69]). Thus, in the $\Gamma_4 - \Gamma_{24}$ RPT region the transversal sound attenuation is determined by the f subsystem attenuation coefficient. Since this latter coefficient is

large, so too will be the former. Moreover, the transversal sound attenuation near this RPT increases due to the presence of a resonance term $\omega_{ac} - \omega_{2df} - \omega_{me5}$ in (4.3).

In $TmFeO_3$, although not all the constants entering (3.1) and (4.4)–(4.7) are known, it is established experimentally that in the $\Gamma_4-\Gamma_{24}$ RPT region $\omega_{20} < \omega_{2f}$ [11, 64], and hence the soft mode at $T = T_1$ is the quasirare-earth mode ω_I (as also evidenced by the line being resolved at $T \approx 100$ K). Its activation at the RPT point is given by (4.5). Using the frequencies from (4.25), the soft mode activation at the RPT point in thulium orthoferrite is $\nu_I(0) \approx 41$ GHz, consistent with the experimental value $\nu_I(0) = 42$ GHz (see Fig. 12).

4.2.2 $\Gamma_2-\Gamma_{24}$ transition on $TmFeO_3$. Near this transition the $\omega_{IV}-\omega_{VI}$ branches (3.33) are virtually identical to the uncoupled branches $\omega_{1f}, \omega_{1k}, \omega_{4k}$. The transversal x-polarised sound is coupled most strongly to the magnetic subsystems. At the RPT point $T = T_2$ the decrease in the velocity of this sound (branch ω_{III}) is limited by the presence of the dipole interaction. Calculation shows that in this case $\tilde{s}_5$ is expressed by (4.12) with $\Lambda = \Lambda_d$. The transversal sound attenuation γ_{III} is determined by Eqn (4.3) in which we replace ω_{ac} (A.4) by ω_{ca} (A.3) and set $\Lambda = \Lambda_d$. Therefore γ_{III} is determined completely by the attenuation in the d subsystem. Thus the rare-earth subsystem near the RPT under study has practically no effect on the velocity and attenuation of sound. This implies that the attenuation coefficient γ_{III} near the $\Gamma_2-\Gamma_{24}$ RPT must be much smaller than near the $\Gamma_4-\Gamma_{24}$ RPT, since in the latter case the sound attenuation is determined by the large attenuation in the f subsystem. Also, the difference in the attenuation of the transversal x-polarised sound may be due to the dipole interaction limiting the resonant term in the denominator in (4.3) for γ_{III} near the $\Gamma_2-\Gamma_{24}$ RPT. Note that this difference in the sound attenuation near the $\Gamma_2-\Gamma_{24}$ and $\Gamma_4-\Gamma_{24}$ transitions may have a consequence that in an $\Gamma_2-\Gamma_{24}$ RPT experiment the sound velocity change will be greater than for $\Gamma_4-\Gamma_{24}$, in spite of the fact that in the former case the magnitude of this change is restricted by the dipole interaction. This is indeed observed experimentally [24] (see Fig. 13).

Thus, we may ignore the attenuation term $(\omega\Lambda)$ when carrying out numerical estimates in (4.12) at frequencies $\lesssim 50$ MHz for the $\Gamma_2-\Gamma_{24}$ RPT. Using data from (4.25) it is found that at $T = T_2$ the fractional velocity change $\Delta s_5/s_5$ must exceed 10%. This agrees to the order of magnitude with the experimental data (see Fig. 13).

The ω_I and ω_{II} branches correspond to the quasiferrous and quasirare-earth modes and are both activation modes at $k = 0$. The magnitude of their activation at the RPT point is given by

$$\omega_I^2(0) = \omega_E(\omega_{me5} + \omega_{dip}) + \omega_{2df}^2 , \tag{4.26}$$

$$\omega_{II}^2(0) = \omega_{2f}^2 - \omega_{2df}^2 \tag{4.27}$$

for $\omega_{20} > \omega_{2f}$, and

$$\omega_I^2(0) = \omega_E(\omega_{me5} + \omega_{dip})\left(1 - \frac{\omega_{2df}^2}{\omega_{2f}^2}\right), \tag{4.28}$$

$$\omega_{II}^2(0) = \omega_{2f}^2 + \omega_E\omega_{me5}\frac{\omega_{2df}^2}{\omega_{2f}^2} \tag{4.29}$$

for $\omega_{20} < \omega_{2f}$.

It is established experimentally that in $TmFeO_3$ the soft mode near the $\Gamma_2-\Gamma_{24}$ RPT is, like in the neighbourhood of $T = T_1$, the quasiferrous mode ω_I [11, 64]. Hence, in this orthoferrite the condition $\omega_{20} < \omega_{2f}$ holds at $T = T_2$, and the soft mode activation is given by (4.28). Comparing (4.28) and (4.5) we see that the soft mode activation near the $\Gamma_2-\Gamma_{24}$ RPT is somewhat smaller that for $\Gamma_4-\Gamma_{24}$ [due to the factor $(1 - \omega_{2df}^2/\omega_{2f}^2)$ in (4.28)]. This is confirmed experimentally in Ref. [11], where the value of activation at $T = T_2$ is measured to be $\nu_2(0) = 40$ GHz (see Fig. 12).

The soft mode activations at $T = T_1$ and $T = T_2$ may also differ due to the difference in the value of F_0, Eqn (3.26), in the Γ_2 and Γ_4 phases, which, in turn, may result from the difference in the d–f exchange contributions to the ferromagnetic moment. For thulium orthoferrite, it is established experimentally [22, 30] that the values of F_0 in the Γ_2 and Γ_4 phases differ by almost a factor of 2.

4.2.3 $\Gamma_2-\Gamma_{12}$ transition in $HoFeO_3$. All the above theoretical results for the $\Gamma_2-\Gamma_{24}$ RPT [i.e., Eqns (4.12), (4.26)–(4.29)] remain valid for this transition if one replaces the indices I, II, and III by IV, V, and VI; 2, 5 by 1, 4; y by x; and sets $\omega_{dip} = 0$ everywhere. It then follows that at $T = T_3$ the transversal y-polarised sound velocity ω_{VI}/k will be reduced much more significantly than for $T = T_1$ or $T = T_2$ (in the ideal non-attenuated case $\omega_{VI}/k \to 0$ as $k \to 0$) because in this case this reduction is not restricted by the dipole interactions (as at $T = T_2$), and because the sound attenuation is determined solely by d subsystem attenuation (at $T = T_1$ the sound attenuation is determined by the large attenuation in the f subsystem). This difference is indeed observed experimentally [13] (see Fig. 15).

Using again the experimental and theoretical results [13, 27–29, 69] on the temperature dependence of the anisotropy constant $K_{cb} = (117.5 - 3T) \times 10^4$ erg cm^{-3} and the sound velocity $\tilde{s}_4$ near the $\Gamma_2-\Gamma_{12}$ transition in $HoFeO_3$, the ME constant B_{44} in this material is estimated to be $B_{44} \approx 4 \times 10^7$ erg cm^{-3}.

For $T = T_3$, (4.22) and (A.5) yield the following estimates for the frequencies entering (3.33):

$$\omega_{1f} \approx 1.4 \times 10^{12}\ \text{s}^{-1}, \quad \omega_{10} \approx 1.2 \times 10^{11}\ \text{s}^{-1},$$
$$\omega_{me4} \approx 3.5 \times 10^7\ \text{s}^{-1}. \tag{4.30}$$

From this we obtain that at the $\Gamma_2-\Gamma_{12}$ point the terms ω_{me4} and $\omega\Lambda$ in (4.2) for $\nu = 50$ MHz are of the same order, and the fractional sound velocity change $\Delta s_4/s_4$ must therefore exceed 10%. That the observed sound velocity reduction is small ($\lesssim 3\%$) is, in our view, explained by two factors. The first is the narrowness of the RPT: to achieve a 50% velocity reduction, one must come very closely (within $\Delta T \sim 10^{-4}$–10^{-3} K) to the RPT point. The second factor is the finiteness of k [the term Dk^2 in (4.12) at $\nu = 50$ MHz is 4×10^4 s^{-1}] and of the attenuation coefficient Λ_d (the term $\omega\Lambda$ at the same frequency is $\approx 1.5 \times 10^4$ s^{-1}).

From (4.30) it follows that the soft mode is the quasiferrous mode ω_{IV}, whose activation is given by (4.28) with $\omega_{dip} = 0$. Thus, the magnitude of activation at $T = T_3$ is mainly determined by the ME coupling and is found to be $\nu_{IV}(0) \approx 16$ GHz. An experimental value of $\nu_{IV}(0)$ is not known because of the lack of two absorption signals [13] (see Fig. 14) due to the large attenuation of the soft mode in question [69].

Based on the study of the ME vibrations in REOFs with non-Kramers rare-earth ions, the following main conclusions are made.

As in REOFs with Kramers f ions, the soft mode near the RPT may be either the d subsystem mode or the f subsystem mode, depending on the ratio of the frequencies of these modes. Thus in $HoFeO_3$, in the $\Gamma_4-\Gamma_{24}$ RPT region the soft mode is the f mode, and near the $\Gamma_2-\Gamma_{12}$ transition, the d subsystem mode. The d subsystem mode frequencies are renormalised by the interaction with the f and elastic subsystems. The soft mode activation at the RPT point tends to exceed the value of the ME gap in the d subsystem vibration spectrum. Apart from the ME coupling, this activation may also be affected by the dipole interaction and by the interactions within the f subsystem and between the d and f subsystems.

The small transversal sound velocity change observed in REOFs with non-Kramers f ions may be attributed to the following mechanisms. In the $\Gamma_2-\Gamma_{24}$ transition region the sound velocity change is small because of the large attenuation in the paramagnetic f subsystem (the absorption line width is of the order of the frequency itself [69]), in terms of which the velocity and the attenuation coefficient of sound are expressed. The attenuation may be so large as to prevent an echo signal in the transition region [24]. Close to the $\Gamma_2-\Gamma_{24}$ and $\Gamma_2-\Gamma_{12}$ RPTs the f subsystem does not contribute to sound attenuation, so that the sound velocity change near these RPTs is much greater than near the $\Gamma_4-\Gamma_{24}$ transition. Near the $\Gamma_2-\Gamma_{24}$ RPT, however, the sound velocity change is limited by the dipole interaction. It should also be noted that the small velocity change near an RPT may also result from the narrowness of the RPT region and the finiteness of k. The same factors may account for the small velocity change near the $\Gamma_2-\Gamma_{12}$ RPT in holmium orthoferrite, even though in this material the dipole interaction does not affect the behaviour of the quasielastic branches.

Again, to confirm the above conclusions and to be able to perform a more detailed comparison of theory and experiment, further data on the ME wave behaviour in REOFs with non-Kramers ions are needed.

4.3 On mechanisms of energy gap formation

In concluding the discussion section, the mechanisms we suggest for the formation of energy gaps at the spontaneous reorientation boundaries will be compared with those proposed in Refs [31–34]. Are these mechanisms mutually exclusive? The model developed in Refs [31–34] involves dissipation and longitudinal magnetisation vibrations, in which case, it is argued, the soft mode is a new, purely relaxational mode, and the soft modes detected in experiment are not actually soft. The corresponding frequency gaps $v \sim (\chi_\parallel/\chi_\perp)^{1/2} H_t$ (where $\chi_\parallel$ and $\chi_\perp$ are respectively the longitudinal and shear susceptibilities of the d sublattice, and H_t is the phase transition field) result from the coupling of the observed modes to the relaxational ones.

We note at this point that the model developed in Refs [7, 25–29] and that of Refs [31, 33] have been verified and substantiated in totally different conditions both in terms of materials and transition types: the former, in experiments on ytterbium, erbium, holmium, and thulium orthoferrites, at spontaneous transitions; the latter, on yttrium and dysprosium orthoferrites and at magnetic-field-induced transitions.

To elucidate the situation, experimental conditions which would suit both the models for a certain REOF were needed. The best candidate for this is $TmFeO_3$, in which the softening quasiferromagnetic resonance branch is closest to its counterpart in $YFeO_3$, a model material from the point of view of the theory of Ref. [31]. An experiment in Ref. [72] carried out for this purpose, measured (as in Refs [31, 33]) the frequency gap at the second-order RPT from the symmetrical phase Γ_2 to the angular phase Γ_{24} in a field **H** along the **a** axis. Owing to the enhanced sample quality, the gap v_2 was narrower than that measured in Ref. [11]. The results of the experiment are presented in Fig. 17 and were obtained on a spherical 0.9-mm-diameter sample in the following manner. First, using the trial record technique described in Ref. [31], the field $\mathbf{H} \parallel \mathbf{a}$ was aligned and fixed as accurately as possible (to within $\sim 0{,}5'$) in the **ac** reorientation plane. Then the temperature dependence of the soft mode frequencies was reconstructed and the corresponding energy gaps at various values of H determined. These latter are indicated under the corresponding temperature points in the figure (together with the transition structure and the geometrical arrangement, the latter being identical to that used in Refs [31, 33]). The main result is that, to the accuracy of the experiment, the gaps v_2 do not depend on the field. This is at variance with the conclusion [31] that the increase in the gap from the spontaneous transition ($H = 0$) to $H = 10$ kOe must be ≈ 8 GHz, much in excess of the gap determination error (± 2 GHz). Thus, the result of Ref. [72] seems at first sight to be in contradiction to the gap formation mechanism suggested in Refs [31, 33]. One can, however, draw a different conclusion from a comparative analysis of the sum total of experimental data for various REOFs. Note that the theory developed in Refs [31, 33] was verified in experiments on $YFeO_3$ and $DyFeO_3$, in which the transition

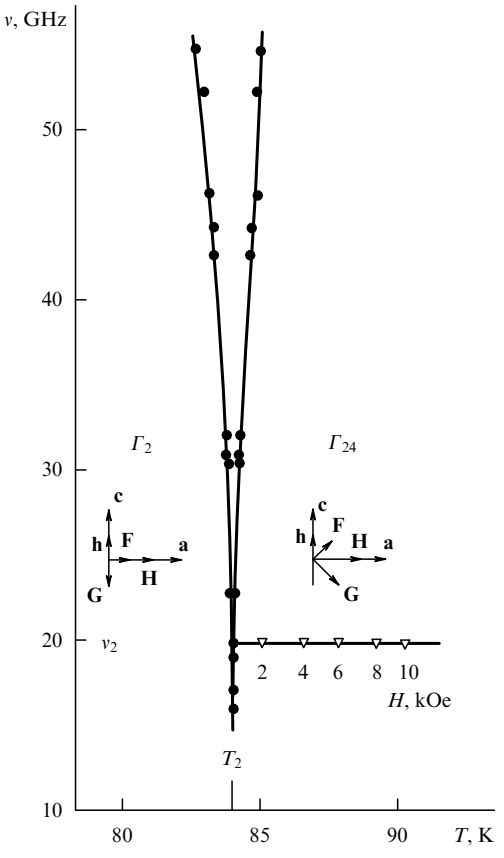

Figure 17. The temperature dependence of the magnetic resonance soft mode at $H = 0$ (●) and of the energy gaps in fields $\mathbf{H} \parallel \mathbf{a}$ equal to 2, 4, 6, 8, and 10 kOe (▽), at $\Gamma_2-\Gamma_{24}$ transition points for $TmFeO_3$; v_2 is the energy gap at the T_2 transition; **h** is the magnetic component of the RF field.

of interest was realised at relatively high temperatures and in a strong magnetic field. A decrease in the 'rigidity' of the iron sublattice at $T \to T_{N1}$ has the consequence that at the upper boundary of the temperature range covered in these experiments (≈ 400 K) the quantity $\chi_\parallel/\chi_\perp$ reaches ≈ 0.5, half the limiting value

$$\left.\frac{\chi_\parallel}{\chi_\perp}\right|_{T=T_{N1}} = 1 .$$

This, together with the large values of the field, brings out clearly the effect of the exchange relaxation mode associated with the longitudinal magnetisation vibrations. However, already at $\chi_\parallel/\chi_\perp \lesssim 0.1$, which corresponds to $T < 100$ K, longitudinal vibrations may contribute negligibly little to the observed gaps as compared to the mechanisms discussed in this review. This is precisely what happens in the experiment in Ref. [72] and in its technologically identical repetitions on $YbFeO_3$ [12] ($T_2 \approx 7$ K) and $ErFeO_3$ [73] ($T_2 \approx 90$ K), which also show the gap to be temperature independent. To summarise, the reported [12, 72, 73] field independence of the gaps is in no conflict with the work of Refs [31, 33], in which the increase of ν_2 with field appears as the most important finding. Most probably, the mechanisms of Refs [31, 33] on the one hand and those discussed here, on the other, dominate in different T and H regions while competing somewhere in between, but contribute additively to the value of the gap. The consistency of the models also follows from the analysis of the dynamics of $ErFeO_3$ near the metamagnetic transition in the rare-earth subsystem [74], with the value of the gap on the second-order transition curve correlating strongly with the longitudinal susceptibility and the field $\mathbf{H} \parallel \mathbf{c}$. For conditions away from the metamagnetic transition ($H = 0$), it has been shown above that the gap at the $\Gamma_2-\Gamma_{12}$ transition point ($T = T_{N2} \approx 4$ K) is explained excellently within the spontaneous transition model discussed.

The general conclusion to be drawn from the comparative analysis above is that for any particular REOF a certain crossover field-temperature region exists in which, taken separately, none of the discussed mechanisms can claim to describe experiment adequately. Sooner or later, a universal approach must emerge in which the dynamics of an orthoferrite, including the nature of the energy gaps, will be described in a single framework for both spontaneous and field-induced transitions.

The first step in this direction was taken in Refs [75, 76] by including the longitudinal susceptibility and magnetisation relaxation in calculating the coupled magnetoacoustic wave spectrum in magnetic materials. The relaxational magnetic mode which in this case would be soft in the absence of ME coupling [31], acquires an activation whose magnitude is determined by this coupling. The soft mode near the RPT now turns out to be the relaxational quasielastic mode. Note also an experiment on the metamagnetic transition in $ErFeO_3$ [77], which reveals a strong correlation between the high-frequency and acoustic characteristics related to longitudinal magnetisation vibrations.

5. Conclusions

By modifying the previous theory, a good qualitative (and in many cases, quantitative) agreement between theory and experiment has been achieved. Unfortunately, given the state of the art of experimentation and single crystal growth technology, no claim for a better adequacy of the experimental and calculated results can be made.

Investigations show that the following factors affect the behaviour (magnitude of the change and frequency dependence) of the sound velocity near the RPT in a particular REOF:

(1) finite (nonzero) wave numbers k used in experiment;

(2) large value of the f subsystem attenuation parameter;

(3) narrowness of the RPT proximity parameter;

(4) the parameters employed in comparing theory and experiment were taken from various studies which used samples prepared of different raw materials, a factor which inevitably affected the final comparison.

The first three factors are particularly important when the ME constants B, and hence the frequencies ω_{me}, are low, which is the situation occurring in REOFs near most of the RPTs considered. In fact, as follows from (4.1), for the sound velocity change to be large the following experimental conditions must be met: $\omega_{me} \gg gK/M_0$, Dk^2, $\omega\Lambda$, and $Dk^2\omega_{me} \gg \omega^2\Lambda^2$. The first condition, for example in erbium orthoferrite near $T = T_1, T_2$, is satisfied only when the RPT 'proximity' $\Delta T = T - T_{1,2} < 2 \times 10^{-3}$ K. The second, in the same material, holds for frequencies $\nu < 60$ MHz, the third (at $\Lambda \approx 6 \times 10^{-3}$), for $\nu < 3$ MHz, and the fourth, for $\Lambda < 3 \times 10^{-4}$. Of these four, only the second, and to some extent the third condition are experimentally realistic. The first and the fourth are very difficult to satisfy. Good candidates are erbium orthoferrites at low temperatures near $T = T_3$ ($\Gamma_2-\Gamma_{12}$ transition), and thulium orthoferrite, both of which have large values of ω_{me}: $\omega_{me4} \approx 10^9$ s^{-1} and $\omega_{me5} \approx 8 \times 10^7$ s^{-1} in the former and the latter, respectively. To these, holmium orthoferrite at $T = T_3$ ($\Gamma_2-\Gamma_{12}$ transition) may probably be added. Among the above materials, erbium orthoferrite at $T = T_3$ enjoys a special position. For it, the above restrictions are $\Delta T < 10^{-1}$ K and $\nu < 6$ GHz, and the condition on Λ is easier to fulfil due to the f subsystem attenuation decreasing significantly at lower temperatures. Presumably this is the reason why this REOF displays an anomalously large sound velocity change of over 25%.

The dispersion of the sound velocity near any RPT is possible only if $gK/M_0 \ll Dk^2$. In erbium orthoferrite near T_1 and T_3, for example, this condition is fulfilled at frequency $\nu = 25$ MHz with $\Delta T < 10^{-6}-10^{-4}$ K. This last condition is even more critical than the one mentioned above. Furthermore, in such a narrow ΔT interval the sound attenuation becomes so large [due to the resonant term in the attenuation expression (4.3)] that echo signals will be absent at all. Experimentally, echo signals disappeared even in a wider interval near the RPT. Presumably, it is for this reason that no sound velocity dispersion has yet been observed in orthoferrites.

There is a further factor to be added to the above four ones affecting the elastic wave velocity behaviour near an RPT, a factor related to misalignment between the wave vector and crystallographic axes. Eqns (4.2) and (4.12) are obtained for $\mathbf{k} \parallel \mathbf{c}$. $\mathbf{k}$ being a little off the axis $\mathbf{c}$ may suppress significantly the sound velocity reduction effect near an RPT [78].

There is a good agreement between the calculated and measured values of the soft quasispin gaps when these latter are d subsystem modes ($\Gamma_2-\Gamma_{24}$ RPT in $ErFeO_3$, and $\Gamma_4-\Gamma_{24}$ and $\Gamma_2-\Gamma_{24}$ RPTs in $TmFeO_3$). This is due to the fact that quite accurate values of d subsystem parameters are available. Unfortunately, no such agreement is observed for the gaps in

the f subsystem soft modes, where the measured and predicted values may disagree severalfold (in ytterbium orthoferrite, for example, by a factor of 4 to 5). A possible explanation is that the exact f subsystem and d – f coupling parameters are not yet known, and in theoretical estimates their approximate values were used.

The authors are grateful to M I Kaganov for helpful discussions and suggestions.

This work has been supported in part by the International Science Foundation and Russian Government through Grant No. JG 9100, the International Science Foundation and Ukrainian Government through Grant No. K6 E100, and by the Ukrainian Fundamental Research Foundation.

Appendix

The contributions to the anisotropy constants (3.10) – (3.12) from the ME and d – f interactions are

$$K_{ac}^{\mathrm{de}} = -\frac{8}{\Delta}\left[B_{11}(B_{11}-B_{31})C_{2233}^2 + B_{12}(B_{12}-B_{32})C_{1133}^2 + B_{13}(B_{13}-B_{33})C_{1122}^2 + (2B_{11}B_{12}-B_{11}B_{32}-B_{12}B_{31})C_{1323}^2 + (2B_{11}B_{13}-B_{11}B_{33}-B_{13}B_{31})C_{1232}^2 + (2B_{12}B_{13}-B_{12}B_{33}-B_{13}B_{32})C_{1213}^2\right] - \frac{B_{55}^2}{c_{55}}, \quad \text{(A.1a)}$$

$$K_{ac}^{\mathrm{df}} = N\left(\frac{B_x^2}{\lambda_3'} - \frac{\lambda_5' B_z'^2 + 2\lambda_7 B_z' B_z'' + \lambda_1' B_z''^2}{\lambda_1'\lambda_5' - \lambda_7^2}\right), \quad \text{(A.1b)}$$

$$K_{20}^{\mathrm{de}} = -\frac{8}{\Delta}\left[(B_{11}-B_{31})^2 C_{2233}^2 + (B_{12}-B_{32})^2 C_{1133}^2 + (B_{13}-B_{33})^2 C_{1122}^2 + 2(B_{11}-B_{31})(B_{12}-B_{32})C_{1323}^2 + 2(B_{11}-B_{31})(B_{13}-B_{33})C_{1232}^2 + 2(B_{12}-B_{32})(B_{13}-B_{33})C_{1213}^2\right] + 2\,\frac{B_{55}^2}{c_{55}}, \quad \text{(A.1c)}$$

$$K_{20}^{\mathrm{df}} = 0, \quad \text{(A.1d)}$$

$$K_{cb}^{\mathrm{de}} = 4\left[(B_{21}-B_{31})u_{xx}^0 + (B_{22}-B_{32})u_{yy}^0 + (B_{23}-B_{33})u_{zz}^0\right] - \frac{B_{44}^2}{c_{44}}, \quad \text{(A.1e)}$$

$$K_{cb}^{\mathrm{df}} = N\left(-\frac{B_y^2}{\lambda_6'} + \frac{\lambda_5' B_z'^2 + 2\lambda_7 B_z' B_z'' + \lambda_1' B_z''^2}{\lambda_1'\lambda_5' - \lambda_7^2}\right). \quad \text{(A.1f)}$$

The characteristic frequencies of the d, f, and elastic subsystems and the interactions between the subsystems are of the following form.

(1) REOFs with Kramers f ions:

(a) Phase Γ_4 [to Eqn (3.19)]

$$\omega_{\alpha k} = s_\alpha k, \quad s_\alpha = \sqrt{\frac{c_{\alpha\alpha}}{\rho}},$$

$$\omega_{\mathrm{me}\alpha} = \frac{g(B_{\alpha\alpha} - B_{\alpha 1}\delta_{\alpha 3})^2}{M_0 c_{\alpha\alpha}} \quad (\alpha = 3,4,5),$$

$$\tilde{\omega}_{2k}^2 = \tilde{\omega}_{\mathrm{E}}\tilde{\omega}_{ac}, \quad \tilde{\omega}_n = \omega_n - \mathrm{i}\omega\Lambda_{\mathrm{d}} \quad (n = \mathrm{E}, ac, cb, ca),$$

$$\omega_{\mathrm{E}} = \frac{gA}{M_0}, \quad \omega_{ac} = \frac{gK_{ac}}{M_0} + \omega_{\mathrm{me}5} + \omega_{2\mathrm{df}} + r\omega_{\mathrm{dip}} + \frac{g\alpha k^2}{M_0},$$

$$r = \left(1 - \frac{v^2k^2}{\varepsilon\omega^2}\right)^{-1}, \quad \omega_{\mathrm{dip}} = 16\pi g M_0 F_0^2,$$

$$\tilde{\omega}_{1\mathrm{f},2\mathrm{f}}^2 = \frac{g^2N^2}{2M_{\mathrm{B}}^2} f_z^2\left\{\tilde{\lambda}_1\tilde{\lambda}_2 + \tilde{\lambda}_4\tilde{\lambda}_5 - 2\tilde{\lambda}_7\tilde{\lambda}_8 \pm \left[(\tilde{\lambda}_1\tilde{\lambda}_2 + \tilde{\lambda}_4\tilde{\lambda}_5 - 2\tilde{\lambda}_7\tilde{\lambda}_8)^2 - 4(\tilde{\lambda}_1\tilde{\lambda}_5 - \tilde{\lambda}_7^2)(\tilde{\lambda}_2\tilde{\lambda}_4 - \tilde{\lambda}_8^2)\right]^{1/2}\right\},$$

$$\tilde{\omega}_{1\mathrm{df}}^3 = \frac{g^3N^3}{M_0M_{\mathrm{B}}^2} f_z^2(\tilde{\lambda}_2 B_z'^2 + 2\tilde{\lambda}_8 B_z' B_z'' + \tilde{\lambda}_4 B_z''^2),$$

$$\tilde{\omega}_{2\mathrm{df}} = \frac{gN}{M_0}\,\frac{\tilde{\lambda}_5 B_z'^2 + 2\tilde{\lambda}_7 B_z' B_z'' + \tilde{\lambda}_1 B_z''^2}{\tilde{\lambda}_1\tilde{\lambda}_5 - \tilde{\lambda}_7^2},$$

$$\tilde{\lambda}_i = \lambda_i' - \frac{\mathrm{i}\omega M_{\mathrm{B}}\Lambda_{\mathrm{f}}}{gN} + 4\pi\mu_i^2 Nr \quad (i = 1,2,4,5),$$

$$\tilde{\lambda}_{7,8} = \lambda_{7,8} - 4\pi\mu_{1,2}\mu_{5,4}Nr,$$

$$\mu_{1,2,3} = \mu_{x,y,z}, \quad \mu_{4,5} = \mu_{xy,yx}. \quad \text{(A.2)}$$

(b) Phase Γ_2 [to Eqns (3.22)]

$$\tilde{\omega}_{1k,2k}^2 = \tilde{\omega}_{\mathrm{E}}\tilde{\omega}_{cb,ca}, \quad \omega_{cb} = \frac{gK_{cb}}{M_0} + \omega_{\mathrm{me}4} + \omega_{1\mathrm{df}} + \frac{g\alpha k^2}{M_0},$$

$$\omega_{ca} = -\frac{g(K_{ac}+K_2)}{M_0} + \omega_{\mathrm{me}5} + \omega_{2\mathrm{df}} + \omega_{\mathrm{dip}} + \frac{g\alpha k^2}{M_0},$$

$$\tilde{\omega}_{1\mathrm{df},2\mathrm{df}} = \frac{gNB_{y,x}^2}{M_0\tilde{\lambda}_{6,3}},$$

$$\tilde{\omega}_{1\mathrm{f},2\mathrm{f}}^2 = \left(\frac{gN}{M_{\mathrm{B}}}\right)^2\tilde{\lambda}_{6,3}\left[\lambda_{1,4}'c_y^2 + \tilde{\lambda}_{5,2}f_x^2 + 2\lambda_{7,8}c_y f_x + 4\pi N(\mu_{1,4}c_y - \mu_{5,2}f_x)^2 r\right],$$

$$\tilde{\lambda}_i = \lambda_i' - \frac{\mathrm{i}\omega M_{\mathrm{B}}\Lambda_{\mathrm{f}}}{gN} + 4\pi N\mu_3^2\delta_{i3} \quad (i = 2,3,5,6). \quad \text{(A.3)}$$

The remaining notation is as in (A.2).

(2) REOFs with non-Kramers ions:

(a) Phase Γ_{24} [to Eqn (3.29)]

$$\tilde{\omega}_{1k,2k}^2 = \tilde{\omega}_{\mathrm{E}}\tilde{\omega}_{ac,ab},$$

$$\omega_{ac} = \frac{2gK_{20}G_x^2G_z^2}{M_0} + \omega_{\mathrm{me}5}(G_x^4 + G_z^4) + \omega_{1\mathrm{df}}G_x^2 + \omega_{\mathrm{dip}}(G_z^2 + rG_x^2) + \frac{g\alpha k^2}{M_0},$$

$$\omega_{ab} = \frac{g(K_{ab} + K_{20}''G_z^2)}{M_0} + \omega_{\mathrm{me}5}G_z^2 + \frac{g\alpha k^2}{M_0},$$

$$K_{ab} = K_{ab}^0 + \frac{d^2}{A} + 4\left[(B_{21}-B_{11})u_{xx}^0 + (B_{22}-B_{12})u_{yy}^0 + (B_{23}-B_{13})u_{zz}^0\right],$$

$$\tilde{\omega}_{1\mathrm{f}}^2 = \tilde{\omega}_{\mathrm{f}}\tilde{\omega}_{\mathrm{f}}', \quad \tilde{\omega}_{\mathrm{f}} = \omega_{\mathrm{f}} - \mathrm{i}\omega\Lambda_{\mathrm{f}}, \quad \tilde{\omega}_{\mathrm{f}}' = \omega_{\mathrm{f}}' - \mathrm{i}\omega\Lambda_{\mathrm{f}},$$

$$\omega_{\mathrm{f}} = 2\Delta_{\mathrm{f}}, \quad \omega_{\mathrm{f}}' = \omega_{\mathrm{f}} - 2\tilde{\lambda}_{\mathrm{f}}f_0\cos^2\psi, \quad \tilde{\lambda}_{\mathrm{f}} = \lambda_{\mathrm{f}} - 4\pi N\mu_1^2 r,$$

$$\omega_{ex} = \frac{g\Delta_{ex}^0 \cos\psi}{5\mu_B}\,, \qquad \omega'_{ex} = \frac{g\Delta_{ex}^0 f_\zeta}{\mu_B}\,, \qquad \omega_{1df} = \frac{\omega_{ex}\omega'_{ex}}{\omega'_f}\,. \tag{A.4}$$

The remaining notation is as before.

(b) Phase Γ_2 [to Eqn (3.32)]: the frequencies ω_{cb} and ω_{ca} are given by (A.3) in which

$$\omega_{1df,\,2df} = 0\,, \qquad \tilde{\omega}_{2f}^2 = \tilde{\omega}_f\,\tilde{\omega}_f''\,, \qquad \omega_f'' = \omega_f - 2\tilde{\lambda}_c f_0 \cos^2\psi\,,$$
$$\tilde{\lambda}_c = \lambda_c - 4\pi N\mu_2^2 r\,, \qquad \omega_{ax,\,ay} = \frac{g\tilde{a}\mu_{1,2}\cos\psi}{5\mu_B}\,,$$
$$\omega'_{ax,\,ay} = \frac{g\tilde{a}\mu_{1,2} f_\zeta}{\mu_B}\,, \qquad \tilde{a} = a - 8\pi M_0 r\,. \tag{A.5}$$

The remaining notation is as before.

References

1. Rudashevsky E G, Shalnikova T A, in *Physics and Techniques of Low Temperatures* (Proc. of 3rd Reg. Conf.) (Prague, 1963) p. 84
2. Tasaki A, Iida S *J. Phys. Soc. Jap.* **18** 1148 (1963)
3. Borovik-Romanov A S, Rudashevskiĭ E G *Zh. Eksp. Teor. Fiz.* **47** 2095 (1964) [*Sov. Phys. JETP* **20** 1407 (1965)]
4. Turov E A, Shavrov B G *Fiz. Tverd. Tela* (Leningrad) **7** 217 (1965) [*Sov. Phys. Solid State* **7** 166 (1965)]
5. Cooper B R *Phys. Rev.* **169** 281 (1968)
6. Turov E A, Shavrov B G *Usp. Fiz. Nauk* **140** 429 (1983) [*Sov. Phys. Usp.* **26** 593 (1983)]
7. Dikshteĭn I E, Tarasenko V V, Shavrov V G *Fiz. Tverd. Tela* (Leningrad) **19** 1107 (1977) [*Sov. Phys. Solid State* **19** 644 (1977)]
8. Vitebskiĭ I M *Zh. Eksp. Teor. Fiz.* **90** 1118 (1986) [*Sov. Phys. JETP* **63** 652 (1986)]
9. Dan'shin N K, Kovtun N M, Sdvizhkov M A *Fiz. Tverd. Tela* (Leningrad) **26** 1200 (1986) [*Sov. Phys. Solid State* **28** 672 (1986)]
10. Dan'shin N K *Fiz. Tverd. Tela* (Leningrad) **30** 1818 (1988) [*Sov. Phys. Solid State* **30** 1045 (1988)]
11. Dan'shin N K, Kramarchuk G G, Sdvizhkov M A, in *Tez. Dokl. 18 Konf. "Fizika Magnitnykh Yavleniĭ"* (Abstracts of Papers Presented at the Eighteenth All-Union Conference on the Physics of Magnetic Phenomena) (Kalinin, 1988) p. 710
12. Dan'shin N K et al. *Zh. Eksp. Teor. Fiz.* **93** 2151 (1987) [*Sov. Phys. JETP* **66** 1227 (1987)]
13. Dan'shin N K et al. *Fiz. Tverd. Tela* (Leningrad) **31** 198 (1989)
14. Balbashov A M et al. *Fiz. Tverd. Tela* (Leningrad) **31** 279 (1989) [*Sov. Phys. Solid State* **31** 1259 (1989)]
15. Vitebskiĭ I M et al. *Zh. Eksp. Teor. Fiz.* **98** 2098 (1990) [*Sov. Phys. JETP* **71** 1179 (1990)]
16. Izotov A I, Tsymbal L T, in *Trudy 15 Vsesoyuznoĭ Konf. "Akustoelektronika i Fizicheskaya Akustika Tverdogo Tela"* (Proceedings of the Fifteenth All-Union Conference on Acoustoelectronics and Physical Solid State Acoustics) (St. Petersburg, 1991) Part 1, p. 73
17. Izotov A I, Tsymbal L T, in *Trudy 19 Vsesoyuznoĭ Konf. "Fizika Magnitnykh Yavleniĭ"* (Proceedings of the Nineteenth All-Union Conference on Physics of Magnetic Phenomena) (Tashkent, 1991) Part 3, p. 47
18. Dan'shin N K, Izotov A I, Tosymbal L T, in *Trudy 19 Vsesoyuznoĭ Konf. "Fizika Magnitnykh Yavleniĭ"* (Proceedings of the Nineteen All-Union Conference on Physics of Magnetic Phenomena) (Tashkent, 1991) Part 3, p. 46
19. Tsymbal L T, Izotov A I *Zh. Eksp. Teor. Fiz.* **102** 963 (1992) [*Sov. Phys. JETP* **75** 525 (1992)]
20. Gorodetsky G, Luthi B *Phys. Rev. B* **2** 3688 (1970)
21. Gorodetsky G, Luthi B, Moran T J *Int. J. Magnetism* **1** 295 (1971)
22. Grishmanovskiĭ A N et al. *Fiz. Tverd. Tela* (Leningrad) **16** 1569 (1974) [*Sov. Phys. Solid State* **16** 916 (1974)]
23. Gorodetsky G, Shtrikman S *J. Appl. Phys.* **51** 1127 (1980)
24. Gorodetsky G, Shaft S, Wanklyn B M *Phys. Rev. B* **14** 2051 (1976)
25. Buchel'nikov V D, Bychkov I V, Shavrov V G *Pis'ma Zh. Eksp. Teor. Fiz.* **54** 467 (1991) [*JETP Lett.* **54** 470 (1991)]
26. Buchel'nikov V D, Bychkov I V, Shavrov V G *Zh. Eksp. Teor. Fiz.* **101** 1869 (1992) [*Sov. Phys. JETP* **74** 999 (1992)]
27. Buchel'nikov V D, Bychkov I V, Shavrov V G *Fiz. Tverd. Tela* (Leningrad) **33** 3439 (1991)
28. Buchel'nikov V D, Bychkov I V, Shavrov V G *Fiz. Nizk. Temp.* **18** 1342 (1992)
29. Buchelnikov V D, Bychkov I V, Shavrov V G *Bull. RAS, Phys. Supplement, Phys. Vibrations* **57** 15 (1993)
30. Mukhin A A, Prokhorov A S *Tr. Inst. Obshch. Fiz. Akad. Nauk SSSR* **25** 162 (1990)
31. Balbashov A M et al. *Zh. Eksp. Teor. Fiz.* **93** 302 (1987) [*Sov. Phys. JETP* **66** 174 (1987)]
32. Balbashov A M et al. *Fiz. Tverd. Tela* (Leningrad) **30** 675 (1988) [*Sov. Phys. Solid State* **30** 386 (1988)]
33. Balbashov A M et al. *Zh. Eksp. Teor. Fiz.* **94** (4) 305 (1988) [*Sov. Phys. JETP* **67** 821 (1988)]
34. Kocharyan K N et al. *Zh. Eksp. Teor. Fiz.* **98** 712 (1990) [*Sov. Phys. JETP* **71** 398 (1990)]
35. Volkov A A et al. *Pis'ma Zh. Eksp. Teor. Fiz.* **39** 140 (1984) [*JETP Lett.* **39** 166 (1984)]
36. Zvezdin A K et al. *Redkozemel'nye Iony v Magnitouporyadochennykh Kristallakh* (Rare-Earth Ions in Magnetically Ordered Crystals) (Moscow: Nauka, 1985)
37. Balbashov A M et al. Preprint IOF Akad. Nauk SSSR No. 97 (Moscow, 1988)
38. Belov K P et al. *Orientatsionnye Perekhody v Redkozemel'nykh Magnetikakh* (Reorientation Transitions in Rare-Earth Magnetic Materials) (Moscow: Nauka, 1979)
39. Hagedorn F B et al. *Phys. Rev. Lett.* **21** 364 (1968)
40. Ozhogin V I et al. *Zh. Eksp. Teor. Fiz.* **62** 2221 (1972) [*Sov. Phys. JETP* **35** 1162 (1972)]
41. Koshizuka N, Hayashi K *J. Magn. Magn. Mater.* **31 – 34** 569 (1983)
42. Balbashov A M et al., in *Tez. Dokl. 18 Konf. "Fizika Magnitnykh Yavleniĭ"* (Abstracts of Papers Presented at the Eighteenth All-Union Conference on the Physics of Magnetic Phenomena) (Kalinin, 1988) p. 720
43. Chernenkov Yu P, Plakhtiĭ V P, Kovalev A V, Preprint LIYaF Akad. Nauk SSSR (Leningrad, 1988)
44. Aring K B, Sievers A J *J. Appl. Phys.* **41** 1197 (1970)
45. Dan'shin N K, Kramarchuk G G, Sdvizhkov M A *Pis'ma Zh. Eksp. Teor. Fiz.* **44** 85 (1986) [*JETP Lett.* **44** 107 (1986)]
46. Bar'yakhtar V G, Vitebskiĭ I M, Yablonskiĭ D A *Zh. Eksp. Teor. Fiz.* **76** 1381 (1979) [*Sov. Phys. JETP* **49** 703 (1979)]
47. Dan'shin N K, Kovtun N M, Sdvizhkov M A *Fiz. Tverd. Tela* (Leningrad) **26** 3635 (1984) [*Sov. Phys. Solid State* **26** 2185 (1984)]
48. White R M, Nemanich R J, Herring C *Phys. Rev. B* **25** 1822 (1982)
49. Barilo S N et al. *Fiz. Tverd. Tela* (Leningrad) **33** 621 (1991)
50. Loewenhaupt M, Sosnowska I, Frick B *J. Phys. Collog.* (France) **49** (C-8), Pt. 2 921 (1988)
51. Barilo S N et al. *Zh. Eksp. Teor. Fiz.* **97** 1921 (1990) [*Sov. Phys. JETP* **70** 1083 (1990)]
52. Kadomtseva A M, Krynetskiĭ I V, Matveev V M *Zh. Eksp. Teor. Fiz.* **79** 1451 (1980) [*Sov. Phys. JETP* **52** 732 (1980)]
53. Klochan V A, Kovtun N M, Khmara V M *Zh. Eksp. Teor. Fiz.* **68** 721 (1975) [*Sov. Phys. JETP* **41** 357 (1975)]
54. Klochan V A et al. *Zh. Eksp. Teor. Fiz.* **81** 627 (1981) [*Sov. Phys. JETP* **54** 335 (1981)]
55. Vitebskiĭ I M et al. *Fiz. Tverd. Tela* (Leningrad) **29** 2738 (1987) [*Sov. Phys. Solid State* **29** 1575 (1987)]
56. Dan'shin N K et al. *Fiz. Tverd. Tela* (Leningrad) **28** 2609 (1986) [*Sov. Phys. Solid State* **28** 1461 (1986)]
57. Dan'shin N K, Kovtun N M, Sdvizhkov M A *Zh. Eksp. Teor. Fiz.* **89** 203 (1985) [*Sov. Phys. JETP* **62** 115 (1985)]
58. Dan'shin N K, Kovtun N M, Sdvizhkov M A *Fiz. Tverd. Tela* (Leningrad) **27** 3635 (1985) [*Sov. Phys. Solid State* **27** 2189 (1985)]
59. Dan'shin N K, Kovtun N M, Sdvizhkov M A *Fiz. Nizk. Temp.* **12** 428 (1986)
60. Dan'shin N K, Kovtun N M, Poluyanenko A P *Zh. Eksp. Teor. Fiz.* **77** 1058 (1979) [*Sov. Phys. JETP* **50** 532 (1979)]
61. Balbashov A M et al., in *Trudy 14 Vsesoyuznoĭ Konf. "Akustoelektronika i Fizicheskaya Akustika Tverdogo Tela"* (Proceedings of the Fourteenth All-Union Conference on Acoustoelectronics and Physical Solid State Acoustics) (Kishinev, 1989) Part 1, p. 150

62. Vitebskiĭ I M et al., in *Tez. Dokl. 26 Vsesoyuznogo Soveshchaniya "Fizika Nizkikh Temperatur"* (Abstracts of Papers Presented at the Twenty-Sixth All-Union Conference on Low-Temperature Physics) (Donetsk, 1990) p. 139
63. Balbashov A M et al. *Pis'ma Zh. Eksp. Teor. Fiz.* **42** 456 (1985) [*JETP Lett.* **42** 564 (1985)]
64. Kozlov G V et al. *Acta Phys. Pol. A* **76** 83 (1989)
65. Shane J R *Phys. Rev. Lett.* **20** 728 (1968)
66. LeCraw R C et al. *J. Appl. Phys.* **39** 1019 (1968)
67. Shapiro S M, Axe J D, Remeika J P *Phys. Rev. B* **10** 2014 (1974)
68. Balbashov A M et al., in *Tez. Dokl. 18 Konf. "Fizika Magnitnykh Yavleniĭ"* (Abstracts of Papers Presented at the Eighteenth All-Union Conference on the Physics of Magnetic Phenomena) (Kalinin, 1988) p. 704
69. Balbashov A M et al. *Zh. Eksp. Teor. Fiz.* **95** 1092 (1989) [*Sov. Phys. JETP* **68** 629 (1989)]
70. Balbashov A M et al. *Pis'ma Zh. Eksp. Teor. Fiz.* **43** 33 (1986) [*JETP Lett.* **43** 41 (1986)]
71. Vitebskiĭ I M, Yablonskiĭ D A *Fiz. Tverd. Tela* (Leningrad) **79** 2300 (1978) [*Sov. Phys. Solid State* **20** 1327 (1978)]
72. Dan'shin N K, Kramarchuk G G *Fiz. Tverd. Tela* (Leningrad) **35** 2586 (1993)
73. Dan'shin N K, Kramarchuk G G, Nepochatykh Yu I *Zh. Eksp. Teor. Fiz.* **105** 660 (1994) [*JETP* **78** 354 (1994)]
74. Dan'shin N K *Fiz. Nizk. Temp.* **20** 353 (1994)
75. Buchel'nikov V D, Shavrov V G *Pis'ma Zh. Eksp. Teor. Fiz.* **60** 534 (1994) [*JETP Lett.* **60** 548 (1994)]
76. Buchel'nikov V D, Shavrov V G *Zh. Eksp. Teor. Fiz.* **106** 1756 (1994) [*JETP* **79** 951 (1994)]
77. Dan'shin N K, Tsymbal L T *Zh. Eksp. Teor. Fiz.* **106** 1765 (1994) [*JETP* **79** 956 (1994)]
78. Buchel'nikov V D, Shavrov V G *Fiz. Met. Metalloved.* **55** 892 (1983)